Approximation by Meshes with Spherical Faces

ANTHONY S RAMOS CISNEROS, KAUST, Saudi Arabia
ALISHER AIKYN, KAUST, Saudi Arabia
MARTIN KILIAN, TU Wien, Austria
HELMUT POTTMANN, TU Wien, Austria / KAUST, Saudi Arabia
CHRISTIAN MÜLLER, TU Wien, Austria

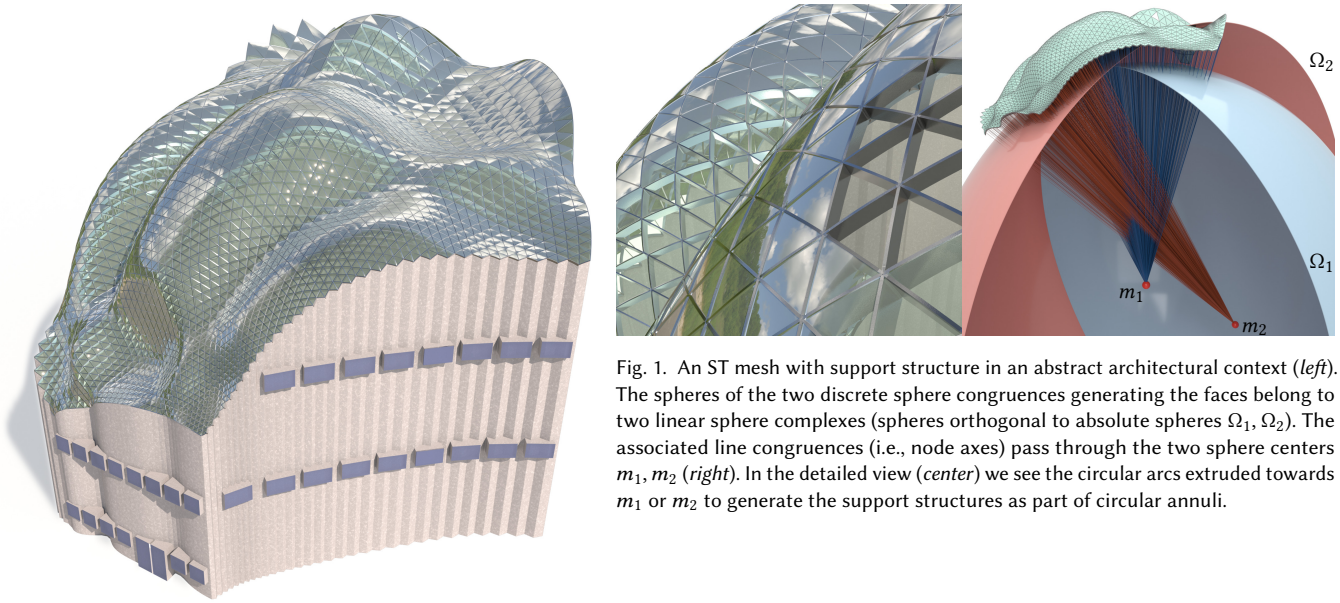

Fig. 1. An ST mesh with support structure in an abstract architectural context (*left*). The spheres of the two discrete sphere congruences generating the faces belong to two linear sphere complexes (spheres orthogonal to absolute spheres Ω_1, Ω_2). The associated line congruences (i.e., node axes) pass through the two sphere centers m_1, m_2 (*right*). In the detailed view (*center*) we see the circular arcs extruded towards m_1 or m_2 to generate the support structures as part of circular annuli.

Meshes with spherical faces and circular edges are an attractive alternative to polyhedral meshes for applications in architecture and design. Approximation of a given surface by such a mesh needs to consider the visual appearance, approximation quality, the position and orientation of circular intersections of neighboring faces and the existence of a torsion free support structure that is formed by the planes of circular edges. The latter requirement implies that the mesh simultaneously defines a second mesh whose faces lie on the same spheres as the faces of the first mesh. It is a discretization of the two envelopes of a sphere congruence, i.e., a two-parameter family of spheres. We relate such sphere congruences to torsal parameterizations of associated line congruences. Turning practical requirements into properties of such a line congruence, we optimize line and sphere congruence as a basis for computing a mesh with spherical triangular or quadrilateral faces that approximates a given reference surface.

CCS Concepts: • **Computing methodologies** → **Shape modeling**.

Additional Key Words and Phrases: discrete differential geometry, architectural geometry, computational design, sphere geometry, sphere mesh, spherical panels

ACM Reference Format:
Anthony S Ramos Cisneros, Alisher Aikyn, Martin Kilian, Helmut Pottmann, and Christian Müller. 2024. Approximation by Meshes with Spherical Faces. *ACM Trans. Graph.* 43, 6, Article 179 (December 2024), 17 pages. https://doi.org/10.1145/3687942

Authors' addresses: Anthony S Ramos Cisneros, anthony.cisneros@kaust.edu.sa, Computer, Electrical and Mathematical Sciences and Engineering Division, KAUST, Saudi Arabia; Alisher Aikyn, alisher.aikyn@kaust.edu.sa, Computer, Electrical and Mathematical Sciences and Engineering Division, KAUST, Saudi Arabia; Martin Kilian, martin.kilian@tuwien.ac.at, Inst. of Discr. Math. and Geometry, TU Wien, Austria; Helmut Pottmann, helmut.pottmann@kaust.edu.sa, Computer, Electrical and Mathematical Sciences and Engineering Division, TU Wien, Austria /, KAUST, Saudi Arabia; Christian Müller, christian.mueller@tuwien.ac.at, Inst. of Discr. Math. and Geometry, TU Wien, Austria.

0730-0301/2024/12-ART179 $15.00
https://doi.org/10.1145/3687942

1 INTRODUCTION

Geometric models composed of spheres arise in numerous applications, including computer graphics, geometric modeling, biology and architecture. Spheres are also basic objects of the classical sphere geometries that deal with sphere preserving transformations and concepts which are preserved under such transformations. An example for an invariant of Möbius sphere geometry is given by the Willmore energy $\int H^2 dA$ (H denoting mean curvature) of surfaces,

which has applications in general relativity, elasticity, cell biology, and surface modeling [Bobenko and Schröder 2005; Canham 1970; Droske and Rumpf 2004; Evans 1974; Hawking 1968; Koerber 2020].

Despite the importance of sphere geometry in diverse applications and the need of efficient discrete representations for computational solutions, there are surprisingly few contributions to discrete sphere geometric surface representations and to discrete sphere differential geometry (see Sec. 1.2). The present paper should also be seen as a contribution to this area.

Motivated by the availability of spherical glass panels in architectural structures, Kilian et al. [2023] presented a study of meshes composed of spherical faces and circular edges. Using concepts of Möbius sphere geometry, they investigated key requirements for applications in architecture, such as a small number of different sphere radii and the availability of a so-called torsion free support structure. This means that the planes of circles through a common vertex pass through a straight line, or equivalently, the spheres of the faces through a common vertex v possess a second intersection point $\bar{v}$. This latter property has an important consequence for the set of spheres that contain the faces: It is a discrete version of a sphere congruence, defined as a two-parameter family of spheres, in which both envelopes are simultaneously represented by a clean mesh with spherical faces.

A support structure is always available for meshes with vertices of valence three, since three pairwise intersecting spheres with one common point have a second intersection point. Thus, spherical hex meshes with regular combinatorics always have a support structure. Spherical triangle (ST) meshes with support structure have a very special geometry; their spheres lie in a so-called linear sphere complex. Spherical quad (SQ) meshes with support structure are discrete counterparts to special unique parameterizations of sphere congruences and play a major role in our paper. We will show how to compute them and how to use them for surface approximation.

1.1 Contributions and Overview

Our main goal is to present algorithms for approximation of a given surface with ST and SQ meshes, focusing on meshes with a torsion-free support structure.

We lay the ground for our approximation algorithms in a discussion of smooth and discrete sphere congruences in Sec. 2. With a sphere congruence, we associate a congruence of lines that connect corresponding contact points on the two envelopes of the sphere congruence (Sec. 2.1). The developable ruled surfaces in this line congruence are an important tool for approximation with meshes that possess a support structure (Sec. 2.2). We show that SQ meshes with support structure are induced by discrete torsal parameterizations of the associated line congruence (Sec. 2.3). ST meshes with support structure have face spheres in a linear sphere complex (Sec. 2.4). In Sec. 2.5, we turn practical requirements into properties of the underlying congruences of spheres and lines. Sec. 2.6 provides further details on the congruence of so-called central spheres, which serve for initialization of optimization algorithms for surface approximation. In each point of a surface f there is a central sphere which has the same mean curvature and the same tangent plane as f, hence good approximation qualities.

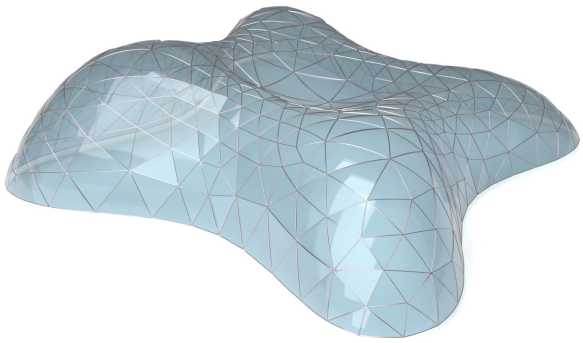

Fig. 2. Size adapted ST mesh obtained by remeshing a reference surface consisting of 3.2k triangles into a mesh with 634 faces. The local face size information of well-fitting spherical patches is determined by keeping the deviation of the sphere mesh from the reference surface below a predefined threshold value $\varepsilon = 0.02$ (see Sec. 3 for details).

It is desirable to adapt the size of spherical faces to the approximation error of the sphere against the given reference surface, cf. Figure 2. This size adaptation forms the content of Sec. 3.

Sec. 4 discusses the highly restricted problem of approximation by ST meshes with support structure.

A core contribution of this paper is the approximation of a given surface with an SQ mesh with support structure (Sec. 5). It requires the computation of an appropriate sphere congruence including properties of the associated line congruence, remeshing by a quad mesh and a final optimization step. Kilian et al. [2023] proposed an algorithm for the computation of an SQ mesh from a given, not optimized sphere congruence. Their remeshing is based on the S^3-model of Möbius geometry, but hard to control in the design space. Our approach does not suffer from such an instability. In comparison with Kilian et al. [2023] the main distinction lies in two essential aspects. First, we focus on approximating given reference surfaces rather than replacing non-spherical faces with spherical ones. And second, to obtain SQ meshes via remeshing strategies, our approach focuses on exploiting associated line congruences (Def. 2.3).

We present our results within Sections 3, 4, 5 and conclude with a discussion of limitations and pointers to future work (Sec. 6).

1.2 Related work

The present paper extends the work of Kilian et al. [2023] by basic geometric insights on sphere congruences and their use in the solution of surface approximation problems. Hence, our literature review focuses on approximation with spheres and underlying concepts from classical and discrete differential geometry.

Classical and discrete differential geometry. Sphere congruences have been studied within differential sphere geometry; we refer to the monographs [Blaschke 1929; Hertrich-Jeromin 2003]. Discrete versions mostly deal with the special case of Ribaucour congruences [Bobenko and Suris 2006; Bobenko and Suris 2007; Bobenko and Suris 2008; Rörig and Szewieczek 2021]. Special nets (parameterizations) are actually objects of sphere geometries. Important examples include principal parameterizations and principal-symmetric nets

[Bobenko and Suris 2007; Bobenko and Suris 2008; Pellis et al. 2020]. Ruled surfaces and line congruences are imporant in several contexts of consistent discretizations. Torsal ruled surfaces, which also appear in our context, are actively investigated (see, e.g., [Verhoeven et al. 2022] and references therein).

The Willmore energy appears in the work of Blaschke [1929] in a study of Möbius geometric counterparts to minimal surfaces. In the special case where the minimizers of the Willmore energy are at the same time isothermic, Thomsen [1924] showed that all surfaces are minimal surfaces. In that case the central spheres are planes. Bobenko and Schröder [2005] presented a discrete Willmore energy for triangle meshes. It possesses a remarkable interpretation as the curvature of a rolling spheres connection determined by the mean curvature spheres [Knöppel et al. 2023]. For a stable and efficient computational approach to the Willmore flow and constrained Willmore surfaces we refer to [Crane et al. 2013; Soliman et al. 2021].

Medial representations and approximation with spheres. The surface c formed by the centers of spheres in a congruence is a bisecting surface of the two envelope sheets $f, \bar{f}$. Such surface-surface bisectors have been studied for example in [Elber et al. 1999; Elber and Kim 2000; Peternell 2000]. The normals to f and $\bar{f}$ meet at c under equal angle and thus reflecting one normal at c yields the other normal. This is used in geometric optics (see e.g. [Pottmann and Wallner 2001, pp 446-450]). In contrast to the above approximation methods, we impose more structure on the family of spheres namely to form a combinatorial mesh with vertices, edges and faces.

Sphere congruences also appear in the construction of the medial axis transform (MAT) of a 3D domain, which views the domain as union of maximal inscribed balls [Amenta et al. 2001; Siddiqi and Pizer 2008]. The set of ball centers is the medial axis. Reconstruction of the domain boundary from the medial axis amounts, for the surface parts of the medial axis, to the computation of the envelopes of a sphere congruence.

Spheres in the MAT are a natural choice for approximation of the boundary of a 3D domain, and they have also been used for deformation, hand modeling and tracking [Stolpner et al. 2012; Thiery et al. 2013, 2016; Tkach et al. 2016]. Medial meshes using sphere-geometric constructions have been proposed for volume approximation [Sun et al. 2013]. Surfaces defined by a union of balls [Edelsbrunner 1993] can serve as models for deformable surfaces and molecular skins [Cheng and Shi 2005; Cheng et al. 2001; Edelsbrunner 1999].

Variational surface approximation using planes, cylinders and spheres has been proposed by Wu and Kobbelt [2005]. Spheres also play a major role in recent work on design rationalization [Jadon et al. 2022]. Wang et al. [2006] presented a variational approach for approximation of an object by a union of spheres for fast collision detection.

2 SPHERE CONGRUENCES FOR APPROXIMATION

Our goal is to approximate a given reference surface f with spherical patches. These spherical patches are part of a discrete family of spheres. To lay the ground of our study we assume for now that the reference surface f is smooth and the discrete family of spheres are contained in a smooth two-parameter family of spheres which are in tangential contact with f.

2.1 Sphere congruences and line congruences

We start with the definition of a sphere congruence, a key notion in our paper.

Definition 2.1. *A* sphere congruence $\mathcal{S}$ *is a (smooth) two-parameter family of spheres $S(u,v)$. Our discretization of a sphere congruence is associated with the combinatorics of a surface-mesh $\mathcal{M}$. We call a discrete family of spheres, where each sphere corresponds to a vertex of $\mathcal{M}$, a* discrete sphere congruence $\mathcal{S}$.

Typical examples of discrete sphere congruences will have the *combinatorics* of $\mathbb{Z}^2$ (as in Fig. 5 right), of a triangle mesh (as in Fig. 5 (left) where the spherical faces are then mainly hexagonal), or of a hexagonal mesh (as in Fig. 10 where the spherical faces are mainly triangular).

A basic task in our approximation problems is the design of an appropriate sphere congruence whose spheres are in tangential contact with the given reference surface f at its points $f(u,v)$. Consequently, such a sphere congruence is determined by the choice of a radius function $r(u,v)$ since the centers are then given by

$$c(u,v) = f(u,v) + r(u,v)\, n(u,v), \tag{1}$$

where n denotes the unit normal vector of f. Hence, a reformulation of our goal is to find a discrete subset of spheres from such a sphere congruence which approximates the reference surface f.

We first focus on the basic geometry and a specific parameterization of sphere congruences (Sec. 2.1) which is essential for our paper. In Sec. 2.2 we discuss the important notion of a support structure and its relation to torsal parametrizations of line congruences (Sec. 2.3). We continue in Section 2.5 with further practical requirements on sphere congruences. Sec. 2.6 deals with an important initial choice of a sphere congruence for our approximation tasks.

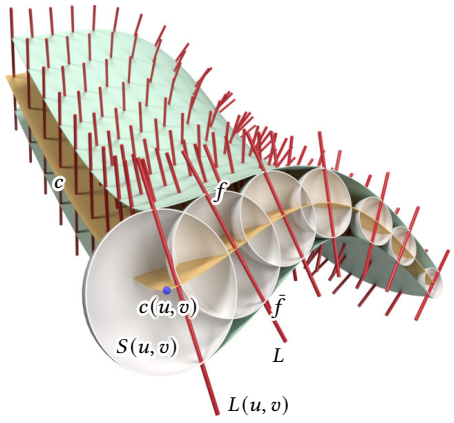

Fig. 3. Sphere congruence $\mathcal{S}$ with associated line congruence. The spheres S are in tangential contact with a reference surface f. Its centers c generate the center surface. Generically there is a second envelope $\bar{f}$ and the lines L connecting the two contact points $f, \bar{f}$ generate the associated line congruence. The lines $L(u,v)$ are orthogonal to the tangent planes of the center surface at $c(u,v)$ but in general $L(u,v)$ does not pass through $c(u,v)$.

Second envelope. We consider a sphere congruence $\mathcal{S}$, formed by spheres $S(u,v)$ with centers $c(u,v)$ and radii $r(u,v)$. In our application, the spheres are tangent to a given surface f at points $f(u,v)$. A sphere congruence $\mathcal{S}$ with a real envelope f has in general a second envelope $\bar{f}$ (for an illustration see Figure 3). The only exception where there is just *one* envelope f are the congruences of principal spheres, i.e., where $r = 1/\kappa_1$ or $r = 1/\kappa_2$ in Equation (1) (see [Blaschke 1929]). Analytically, the envelopes can be computed by intersecting three surfaces:

Lemma 2.2. *Let $\mathcal{S}$ be a sphere congruence where the spheres $S(u,v)$ have the implicit representation equations*

$$s(u,v,x) := \|x - c(u,v)\|^2 - r(u,v)^2 = 0.$$

Then the points $f(u,v)$, $\bar{f}(u,v)$ on the envelope are the intersection points of the sphere $S(u,v)$ with the two "partial derivative" planes S_u, S_v with equations $s_u = s_v = 0$, i.e.,

$$S_u : \langle x - c, c_u\rangle + r r_u = 0, \quad S_v : \langle x - c, c_v\rangle + r r_v = 0. \tag{2}$$

For a proof see e.g. [Pottmann and Peternell 2000]. There is a possibility that a sphere congruence has no real envelope in the case where the three surfaces S, S_u, S_v do not intersect in real points.

Associated line congruence. There is an important relation between sphere congruences and two-parameter families of lines which will also play an important role in our theory as well as in our optimization strategy later on.

Definition 2.3. *A* (general) line congruence *is a two-parameter family of straight lines. We call the line congruence $\mathcal{L}$* associated line congruence *of $\mathcal{S}$ if its lines $L(u,v)$ connect corresponding contact points $f, \bar{f}$ of the sphere congruence $\mathcal{S}$.*

The lines $L(u,v)$ of the associated line congruence equal the intersection $S_u \cap S_v$ of the derivative planes (2). Since f and $\bar{f}$ fulfill the equation of the plane S_u we have

$$\langle f - c, c_u\rangle + r r_u = 0 \quad \text{and} \quad \langle \bar{f} - c, c_u\rangle + r r_u = 0.$$

Subtracting these equations yields $\langle f - \bar{f}, c_u\rangle = 0$. Analogously we have $\langle f - \bar{f}, c_v\rangle = 0$. Consequently, $f - \bar{f}$ is orthogonal to c_u and c_v, i.e., the line L is orthogonal to the tangent plane of the *center surface* $c(u,v)$ (cf. Fig. 3). Furthermore, the computation of contact points $f(u,v)$, $\bar{f}(u,v)$ also shows that they are symmetric with respect to the tangent plane of the center surface at $c(u,v)$.

Channel surfaces in a sphere congruence. For better visualization of the underlying concepts we also consider the images of curves $(u(t), v(t))$ in the parameter domain of a sphere congruence. In this way we obtain a one-parameter family of spheres which envelopes a so called *channel surface* (see Fig. 4). In particular, *isoparameter channel surfaces* are enveloped by $s(u(t), v_0)$ or $s(u_0, v(t))$ for constant u_0, v_0. A sphere $S(u(t), v(t))$ touches the channel surface along a circle in the derivative plane given by

$$0 = \frac{d}{dt} s(u(t), v(t), x) = \dot{u} s_u + \dot{v} s_v,$$

where $\dot{u} = \frac{d}{dt} u$. Such a circle is called *characteristic circle* of the channel surface. For each t the characteristic circle also contains the enveloping points $f(u(t), v(t))$, $\bar{f}(u(t), v(t))$. The channel surface is in tangential contact to both envelopes $f, \bar{f}$ at these enveloping points. The connecting lines $L(u(t), v(t))$ of these corresponding enveloping points form the *associated ruled surface* corresponding to the channel surface (see Fig. 4). The associated ruled surface is part of the associated line congruence $\mathcal{L}$ and is in general not developable. However, the cases where the associated ruled surface *is* developable will turn out to be important for us.

Discrete sphere congruence. A *discrete sphere congruence* is a discrete family of spheres associated with the combinatorics of a surface-mesh $\mathcal{M}$. There is a sphere per each combinatorial vertex of $\mathcal{M}$. However, the concept of an envelope of a discrete sphere congruence differs a little bit from its smooth counterpart since we have no continuous limits. The following definition aligns with the one from [Kilian et al. 2023].

Definition 2.4. *A sphere congruence corresponding to a combinatorial mesh $\mathcal{M}$ has a* discrete envelope *if the spheres corresponding to a face of $\mathcal{M}$ intersect in a point. The* discrete envelope *is then a sphere mesh consisting of spherical patches as faces and circular arcs as edges. The combinatorics of the sphere mesh is dual to the given combinatorics $\mathcal{M}$ of the sphere congruence (see e.g., Fig. 5 (left) which is a hexagon-dominant sphere mesh whose underlying combinatorics $\mathcal{M}$ is triangular).*

Hence, the discrete sphere congruence envelopes a sphere mesh if the spheres which belong to a face of the congruence pass through a common point v. The envelopes of two different sphere congruences are illustrated in Figure 5. The property in the smooth case where the existence of one envelope implies the existence of a second envelope, does not carry over to the discrete setting. However, the presence of a second envelope characterizes the existence of a so called support structure (see Sec. 2.2).

2.2 Sphere congruences with support structures

Support structure. The following discussion is important for the computation of sphere meshes with a torsion-free support structure. This is particularly important for quadrilateral sphere meshes which we call *SQ meshes*; see Sec. 5. The basic properties have been

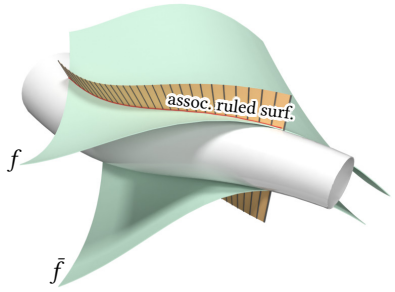

Fig. 4. The envelope of a one-parameter family of spheres is a channel surface. The channel surface which is enveloped by a one-parameter family of spheres from a sphere congruence is in tangential contact with the two envelopes $f, \bar{f}$ along two contact curves. The associated ruled surface connects corresponding contact points precisely where the spheres generating the channel surface touch the envelopes.

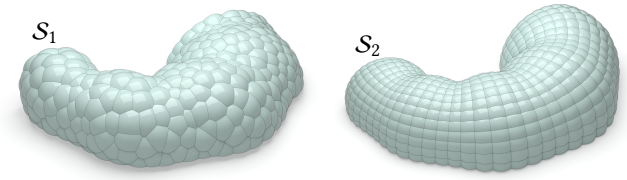

Fig. 5. The sphere congruence $\mathcal{S}_1$ (*left*) corresponds combinatorially to a triangle mesh $\mathcal{M}_1$, i.e., there is a sphere for each vertex of the triangle mesh $\mathcal{M}_1$. Three spheres belonging to a combinatorial face F of $\mathcal{M}_1$ intersect in two points implying that $\mathcal{S}_1$ has two envelopes (a visible outer one and an invisible inner one). The envelope is a sphere mesh with generically hexagonal sphere patches as faces. The sphere congruence $\mathcal{S}_2$ (*right*) corresponds combinatorially to a quad mesh $\mathcal{M}_2$, i.e., there is a sphere for each vertex of the quad mesh $\mathcal{M}_2$. Four spheres belonging to a combinatorial face F of $\mathcal{M}_2$ intersect in a point implying that $\mathcal{S}_2$ has an envelope, the visible outer sphere mesh which is also a quad mesh, but with spherical faces and circular arcs as edges. There is not necessarily a second envelope.

discussed already by Kilian et al. [2023], but in connection with the representation in the point model of Möbius geometry. In view of the computational approach in Section 5, we focus on the associated line congruence (Def. 2.3).

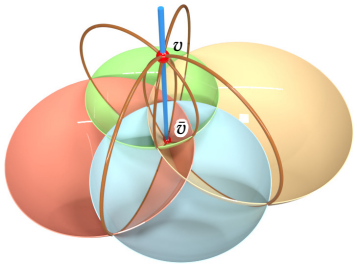

Fig. 6. Four spheres pass through two points $v, \bar{v}$. They form a node suitable for a support structure. The connecting line $v\bar{v}$ (blue) belongs to the associated line congruence.

A sphere mesh has a *support structure* if the spheres with a common vertex v pass through a second common point $\bar{v}$, which can be considered a point of the discrete second envelope. The connecting line $v\bar{v}$ of the two discrete envelope points is the *node axis*; see Fig. 6. It is a member of the *discrete associated line congruence*. The planes in which the circular edges around a vertex v are lying pass through this node axis.

Two neighboring node axes lie in the plane of the common circular edge and thus intersect. The collection of all node axes forms a *discrete line congruence*. A sequence of neighboring node axes together with the planes that connect these neighboring axes forms a discrete developable surface (see Fig. 7). It therefore forms a so called *torsal parameterization* of the *discrete line congruence*.

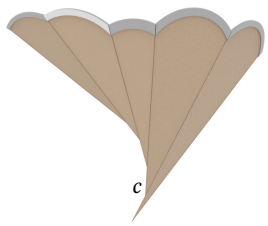

Fig. 7. A sequence of neighboring node axes together with the planes that connect these neighboring axes forms a discrete developable surface. The axes envelope a discrete space curve c.

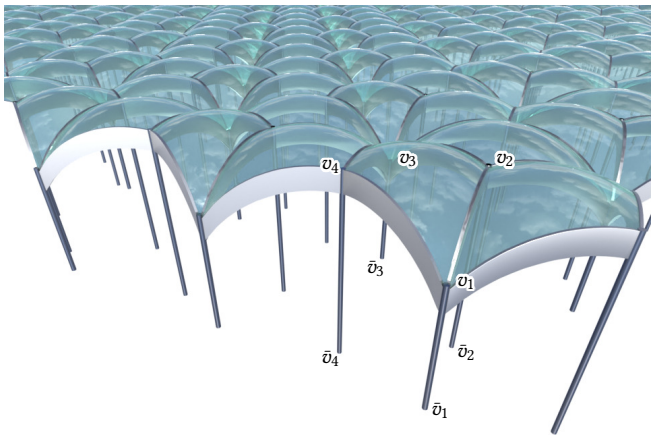

Fig. 8. Hexahedral cells of an SQ mesh with a torsion-free support structure. The vertices of the four "vertical" faces of each cell are planar and circular whereas the vertices of the two "horizontal" faces (the upper one of them rendered as glass panel) are not even planar.

In this way, an SQ mesh with a support structure defines a discrete structure formed by hexahedral cells (Fig. 8) in which four of the six faces are planar (vertical faces in Fig. 8). Their planes intersect in four edges, the node axes. The vertices of the other two faces are in general not planar (like the glass-style rendered faces in Fig. 8). However, all eight vertices lie on a common sphere s_{ij}, an element of the discrete sphere congruence. If the cells are free of self-intersections, we obtain a cell packing structure in the sense of [Pottmann et al. 2015], which tiles the space between the two envelopes of the sphere congruence.

Since four spheres through two common points $v, \bar{v}$ (=node axis) have their centers in the bisecting plane of $v, \bar{v}$, the quad mesh of sphere centers has planar faces, and each pair of vertices $v, \bar{v}$ on the two envelopes is symmetric with respect to the corresponding face of the center mesh.

R-congruences. If one envelope of a quadrilateral sphere congruence with two envelopes has circular faces, i.e., the vertices of the spherical face lie in a plane (unlike in Figure 8), then so does the second envelope. This is an immediate consequence of Miquel's theorem which can be formulated as follows:

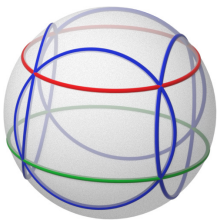

If a combinatorial cube has its eight vertices on a sphere and if five of the six faces are planar, then the sixth face is planar as well. As a consequence, if the vertices of one of the two enveloping meshes form a circular mesh (i.e., a *discrete principal parameterization*), the same is true for the other discrete envelope. In this case, we have a so-called discrete *R-congruence*. The geometry of these congruences has recently been studied in detail [Rörig and Szewieczek 2021], but we are not aware of computational design approaches.

2.3 Torsal parametrizations of the line congruence

The smooth counterparts to the sequences of coplanar node axes along discrete parameter lines are developable ruled surfaces in the associated line congruence $\mathcal{L}$. Hence, the smooth analog of a discrete sphere congruence with $\mathbb{Z}^2$ combinatorics and with support structure is a smooth sphere congruence with an associated line congruence given as so-called *torsal parameterization*. This means that both families of iso-parameter ruled surfaces in the congruence are developable (see, e.g., [Pottmann and Wallner 2001]). The tangent planes of these developable ruled surfaces in $\mathcal{L}$ are called *torsal planes*. Analytically, a direction $(\dot{u}, \dot{v})$ in the u, v parameter plane defines a torsal direction of the sphere congruence at (u, v) if

$$\det(\dot{u} f_u + \dot{v} f_v, l, \dot{u} l_u + \dot{v} l_v) = 0, \tag{3}$$

with $l = c_u \times c_v$ as direction vectors of $L(u, v)$. The three vectors in the determinant span the torsal plane. Equation (3) is a homogeneous quadratic equation in $(\dot{u}, \dot{v})$, with zero, one or two real solutions. Only the case with two real solutions is of interest to us.

Even though the notion of a line congruence is not a concept of Möbius geometry, a torsal parametrizations of the associated sphere congruence is preserved under Möbius transformations.

Lemma 2.5. *Consider a torsal parametrization $L(u, v)$ of the associated line congruence of a sphere congruence $S(u, v)$. The associated line congruence corresponding to the sphere congruence obtained by applying a Möbius transformation to the spheres $S(u, v)$ is again in torsal parametrization. (Note that the Möbius transformation is not applied to the developable surfaces in the line congruence.)*

Proof. A torsal plane τ in u-direction at (u, v) passes through the line $L(u, v)$, i.e., through $f(u, v)$ and $\bar{f}(u, v)$, and is parallel to $f_u(u, v)$ and $\bar{f}_u(u, v)$. This plane τ intersects the sphere $S(u, v)$ along a circle $k^u(u, v)$. We can therefore also say that τ is spanned by $k^u(u, v)$. A Möbius transformation maps the circle $k^u(u, v)$ to a circle which spans the torsal plane of the associated line congruence of the transformed sphere congruence. This follows from the fact that contact points $f, \bar{f}$ are mapped to contact points and tangency of curves is preserved by Möbius transformations. □

Smooth principally parametrized sphere congruence. A smooth sphere congruence with centers $c(u, v)$ and radii $r(u, v)$ is called *principally parametrized*, if c and $\rho := \|c\|^2 - r^2$ satisfy

$$c_{uv} = a c_u + b c_v \quad \text{and} \quad \rho_{uv} = a \rho_u + b \rho_v, \tag{4}$$

for some real valued functions $a = a(u, v)$, $b = b(u, v)$ (cf. [Bobenko and Suris 2008, p. 20]).

Lemma 2.6. *The parametrization of the associated line congruence $\mathcal{L}$ of a principally parametrized sphere congruence $\mathcal{S}$ is torsal.*

Proof. The second equation of (4) implies

$$\langle c_u, c_v \rangle - r_u r_v - r r_{uv} + a r r_u + b r r_v = 0. \tag{5}$$

Differentiating by u the second equation of (2), which is satisfied for $x = f$ and $x = \bar{f}$, implies

$$\langle c_v, c_u - f_u \rangle + \langle c_{uv}, c - f \rangle = r_u r_v + r r_{uv}$$

and using the first equation of (4) yields

$$\langle c_v, f_u \rangle - \langle c_u, c_v \rangle + r_u r_v + r r_{uv} - a \langle c_u, c - f \rangle - b \langle c_v, c - f \rangle = 0.$$

Using Equations (2) and (5) yields $\langle c_v, f_u \rangle = 0$. Analogously, we get $\langle c_u, f_v \rangle = 0$ and also for $\bar{f}$, i.e., $\langle c_v, \bar{f}_u \rangle = \langle c_u, \bar{f}_v \rangle = 0$.

Furthermore, Equations (2) imply $\langle c_u, f - \bar{f} \rangle = \langle c_v, f - \bar{f} \rangle = 0$. Consequently, we have $\langle c_v, f_u \rangle = \langle c_v, \bar{f}_u \rangle = \langle c_v, f - \bar{f} \rangle = 0$ which implies that $f - \bar{f}, f_u, \bar{f}_u$ are coplanar and therefore the u-ruled surfaces $L(u, v_0)$ are developable. Analogously, the v-ruled surfaces $L(u_0, v)$ are developable. □

Remark 2.7. The opposite direction is not true, i.e., a torsal parametrization is not necessarily induced by a principal parametrization. This follows from a simple counterexample: $c(u, v) = (u, u+v, 0)$ and $r(u, v) = 1$. Here we have $c_u = (1, 1, 0)$, $c_v = (0, 1, 0)$ and therefore $0 = c_{uv} = 0c_u + 0c_v$ but $\rho_{uv} = 2$ which contradicts Equations (4).

We call the isoparameter channel surfaces in a principal parameterization $s(u, v)$ the *principal channel surfaces*; they form a counterpart to the principal curvature lines of a surface. Reformulating the above insights, we can state: *The associated ruled surface along a principal channel surface in a sphere congruence is developable.*

Principal channel surfaces in an R-congruence touch the envelopes $f, \bar{f}$ along their principal curvature lines.

2.4 Sphere congruences in a linear sphere complex

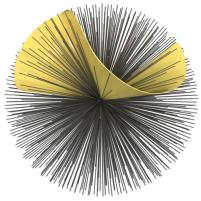

The special case of a line congruence, which is particularly important for ST meshes with a support structure, consists of all lines in $\mathbb{R}^3$ through a fixed point m. Such a family of lines is called *(line) bundle*. Every curve in the parameter domain of such a line bundle $\mathcal{L}$ parametrizes a cone with vertex m which is therefore a developable ruled surface.

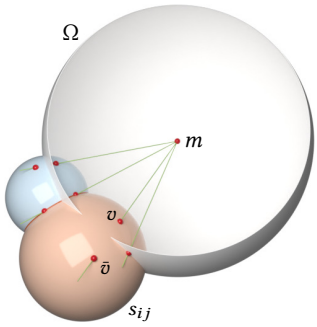

Let us now consider a discrete sphere congruence $\mathcal{S}$ whose associated line congruence is the line bundle $\mathcal{L}$. The line connecting the two contact points $v, \bar{v}$ of any sphere $s_{ij} \in \mathcal{S}$ with its two envelopes passes through m. The *power* of m with respect to the sphere s_{ij} is the real number $R^2 := \overline{mv} \cdot \overline{m\bar{v}}$. That number R^2 is the same for any two intersection points with a line through m. The sphere Ω with center m and squared radius R^2 is orthogonal to s_{ij}. Since adjacent cells have common vertex pairs, that radius R of Ω is constant over the entire structure which implies:

Lemma 2.8. *The sphere congruence $\mathcal{S}$ whose associated line congruence $\mathcal{L}$ is a line bundle is formed by all spheres which are orthogonal to a sphere Ω. The spheres of $\mathcal{S}$ lie in a so called* linear sphere complex.

This special case of a line congruence appears for ST meshes with a support structure in Sec. 4. For that the sphere Ω can be real, imaginary or degenerate to a point. We discuss the three cases in Sec. 2.6. An example with a real sphere Ω can be found, e.g., in Fig. 9.

In the case where $R = 0$ all spheres of $\mathcal{S}$ pass through a fixed point m. One of the two envelopes $f, \bar{f}$, say $\bar{f}$, degenerates to the point $\bar{f} = m$. Assuming m being the origin of coordinates, any conjugate

parametrization of the center surface c yields a principally parametrized sphere congruence as then c together with $\rho = \|c\|^2 - r^2 \equiv 0$ fulfill Equations (4). Geometrically, this case is best understood after applying a Möbius transformation ι, more precisely, an inversion in a sphere with center m, that maps m to ∞. All spheres of $\mathcal{S}$ are mapped to tangent planes of the surface $\iota(f)$. The channel surfaces in the congruence are mapped to tangent developable surfaces of $\iota(f)$. The characteristic circles of the channel surface are mapped to the rulings of the tangent developable surface.

Note that a sphere congruence $\mathcal{S}$ which lies in a linear complex with $R^2 > 0$ has two envelopes which correspond to each other in the inversion with respect to the sphere Ω. See Figure 10 for a pair of ST meshes lying inverse with respect to a real sphere Ω. Since curvature lines are invariant under Möbius transformations and since the two envelopes are inverse images of each other, also the curvature lines correspond to each other by virtue of the sphere congruence. Therefore such a congruence is an R-congruence. Furthermore, since the inversion is a conformal map the two envelopes are related by a conformal structure preserving R-congruence (i.e., they are related by a so called *Darboux transformation*). In applications with larger meshes with larger shape variations we might not have a single absolute sphere but utilize fabrication tolerances and obtain ST meshes with face spheres belonging to several absolute spheres as illustrated in Fig. 1.

2.5 Requirements on sphere congruences for good approximations

Given a reference surface $f(u, v)$, there is a sphere congruence for every real function $r(u, v)$ determining the radii and hence the sphere centers via Equation (1). However, not all sphere congruences are good from a practical point of view, e.g., for fabrication or visual appearance. Important conditions for all of our applications are the following: (a) the spheres of the mesh should locally approximate the surface well, (b) the support structure should locally lie rather transversally and less tangentially to the reference surface, and (c)

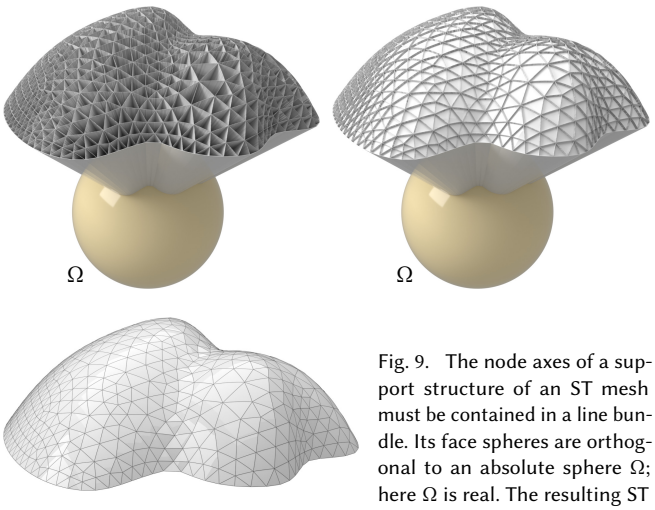

Fig. 9. The node axes of a support structure of an ST mesh must be contained in a line bundle. Its face spheres are orthogonal to an absolute sphere Ω; here Ω is real. The resulting ST mesh is reasonably smooth compared to the same surface optimized just for smoothness without support structure (Fig. 12, 15).

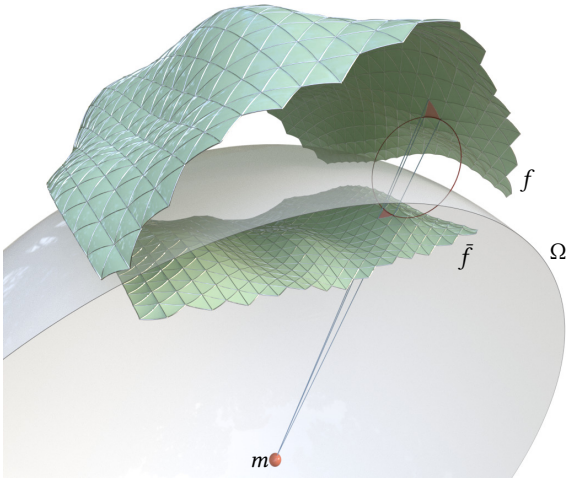

Fig. 10. Two ST meshes $f, \bar{f}$ with support structure. The sphere Ω is real in this case and the two envelopes $f, \bar{f}$ are related by an inversion in Ω. Both ST meshes are polyhedral surfaces in hyperbolic space.

the intersection angles of the discrete parameter lines should not deviate too much from 90 degrees or at least in a controllable way. We now go into more details and formulate the property statements for later reference:

(a) The spheres $s(u, v)$ shall be good local approximations of the given surface f at $f(u, v)$.

We will elaborate on spheres with good approximation qualities in more details in Section 2.6.

We also want neighboring spheres $s(u, v)$ and $s(u + \Delta u, v + \Delta v)$ to intersect in a circle whose plane forms an angle $\nu \in [0, \theta]$ with the surface normal $n(u, v)$ at $f(u, v)$ for some given threshold θ. The intersection of two spheres lies in a plane which is orthogonal to the connecting line of sphere centers $c(u, v)$ and $c(u+\Delta u, v+\Delta v)$. These connections are close to tangents of the center surface c of $\mathcal{S}$. Thus, the angle threshold θ implies a threshold on the angle μ between the normals $n(u, v)$ of f and the normals of the center surface $c(u, v)$. If n is close to the direction of L, which is what we want, then also μ and ν are close. Consequently, for small θ the two angle thresholds are close. The lines L of the associated congruence are orthogonal to the tangent planes of the center surface c. Consequently, the angle between L and n should not exceed the threshold θ. Hence, for SQ meshes with support structure, (b) is a natural practical requirement on the node axes:

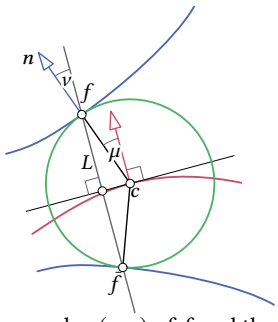

(b) At each point $f(u, v)$ of the given surface, the normal $n(u, v)$ and the line $L(u, v)$ of the associated line congruence $\mathcal{L}$ form an angle ν that should not exceed a given threshold θ.

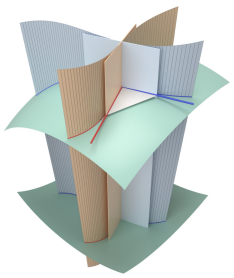

In Section 5, we will compute a sphere congruence $\mathcal{S}$ such that its associated line congruence $\mathcal{L}$ contains two families of developable ruled surfaces that meet at the lines L of $\mathcal{L}$ under a suitable angle. This angle is measured as angle between their tangent planes, the so-called *torsal planes* of lines L. Ideally, these planes should form an angle with a prescribed maximum deviation from $\pi/2$. Equally important is the intersection angle between the so-called *torsal directions on* f which are the directions of the intersection curves of the developable ruled surfaces with f. We obtain the same directions from the intersection lines of the tangent plane at $f(u,v)$ and the torsal planes through $L(u,v)$. By symmetry the same angle is measured at the second envelope $\bar{f}$. The closer the line L is to the normal vector n the closer is the angle between the torsal directions and the angle between the torsal planes. In summary, we have:

(c) The line congruence $\mathcal{L}$ associated to the sphere congruence $\mathcal{S}$ shall have torsal directions on f with a prescribed maximum deviation from $\pi/2$.

Note the following relation between properties (b) and (c). If (b) is fulfilled with $\theta = 0$, the associated line congruence $\mathcal{L}$ is the common normal congruence of the surfaces f and $\bar{f}$. All spheres have a constant radius and $f, \bar{f}$ form a pair of offset surfaces. The developable surfaces in the normal congruence $\mathcal{L}$ are formed by the normals along principal curvature lines of f and $\bar{f}$ and the torsal planes are orthogonal. Hence, also (c) is optimally satisfied. The converse is not true, as we see by applying a Möbius transformation. Right angles between torsal directions on f are preserved, but the angle between torsal planes will in general no longer be $\pi/2$. R-congruences always optimally fulfill (c), since the torsal directions on f and $\bar{f}$ are principal curvature directions.

2.6 The congruence of central spheres

We are now looking for a sphere congruence with a high approximation quality at surface points. For each tangent direction the sphere with the inverse normal curvature (the Meusnier sphere) is the best approximating sphere in that direction. The extreme normal curvatures at a surface point are the principal curvatures κ_1 and κ_2. Their arithmetic mean $H = \frac{1}{2}(\kappa_1 + \kappa_2)$, i.e., the *mean curvature*, is by definition an averaging curvature at a surface point. A sphere in tangential contact with a surface f at a specified point $f(u,v)$ and with $1/H$ as radius can therefore be seen as a well approximating sphere at $f(u,v)$.

Definition 2.9. *The* central sphere *or* mean curvature sphere *at a surface point $f(u,v)$ has the center $c(u,v) = f(u,v) + \frac{1}{H(u,v)} n(u,v)$ and radius $1/H(u,v)$, where n is a unit normal vector at f.*

The central sphere and f share the common tangent plane and the mean curvature at $f(u,v)$. Thus, the central sphere congruence $\mathcal{S}_c$ has good local approximation qualities (property (a)). It is furthermore important in differential geometry of spheres [Blaschke 1929] as well as in our paper.

Let us compute the associated line congruence $\mathcal{L}$ of the central sphere congruence $\mathcal{S}_c$ for a general surface f. We use a curvature line parameterization of f (which always exists away from umbilics). It is characterized by Rodrigues' formulas $n_u = -\kappa_1 f_u$, $n_v = -\kappa_2 f_v$ [do Carmo 1976, p. 145]. The tangent plane of the center surface c is spanned by

$$c_u = -\sigma f_u - \frac{H_u}{H^2} n, \quad c_v = \sigma f_v - \frac{H_v}{H^2} n, \quad \text{where} \quad \sigma = \frac{\kappa_1 - \kappa_2}{\kappa_1 + \kappa_2}.$$

The lines L in $\mathcal{L}$ have direction vectors $c_u \times c_v$. In the principal frame at $f(u,v)$ with basis vectors $e_1 = f_u/\|f_u\| = f_u/\sqrt{E}$, $e_2 = f_v/\|f_v\| = f_v/\sqrt{G}$, and $n = e_1 \times e_2$, they read

$$c_u \times c_v = \frac{\sigma H_u \sqrt{G}}{H^2} e_1 - \frac{\sigma H_v \sqrt{E}}{H^2} e_2 - \sigma^2 \sqrt{EG}\, n.$$

Using the so-called *invariant directional derivatives in principal directions* of H which read $H_{,1} := H_u/\sqrt{E}$ and $H_{,2} := H_v/\sqrt{G}$ (cf. [Blaschke 1930, Chap. 5] and scaling with $H^2/(\sigma\sqrt{EG})$ the cross product $c_u \times c_v$ becomes

$$l(u,v) := (H_{,1}, -H_{,2}, -\sigma H^2) = \big(H_{,1}, -H_{,2}, \frac{\kappa_2^2 - \kappa_1^2}{4}\big),$$

represented in the principal frame.

Example 2.1. At a point (u,v) where H is stationary $l(u,v)$ equals $(0,0,*)$, hence L is a surface normal. This happens for example at all points of a surface with constant $H \neq 0$ (CMC surface).

Example 2.2. At umbilical points we have $\kappa_1 = \kappa_2$ and thus L is a surface tangent if H is not stationary. At umbilical points where H is also stationary – this, for example, is the case at all points of a sphere f – the lines L are not defined since f is identical with all central spheres, but in that case our approximation task is trivial anyway.

Example 2.3. The normal component of l also vanishes at points with $H = 0$. For a minimal surface, i.e., $H = H_{,1} = H_{,2} = 0$, the vector l vanishes. There, the central spheres are the tangent planes, and they do not have a second envelope.

Given a surface f, the computation of central spheres involves second derivatives, the line congruence third derivatives, and the identification of torsal directions via Equation (3) fourth derivatives of f. Thus the computation of torsal directions is involved, and we therefore omit it here. However, we add some practical implications and show below that for some important surface classes torsal directions of the central sphere congruence are orthogonal. Examples with no real torsal directions are general Willmore surfaces where they are always imaginary.

For the practical computation of torsal directions we realize that fourth order derivatives render a completely discrete approach impractical, as regularization becomes less feasible. We therefore use a spline representation of f and of an (approximate) central congruence $\mathcal{S}_c$ and only in later stages apply a discrete sampling to optimize the congruence so that it satisfies properties (a), (b) and (c); see Section 5.

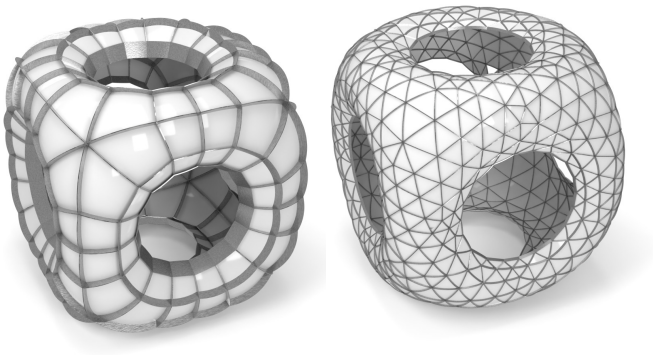

Fig. 11. Sphere meshes as discrete minimal surface in hyperbolic space. *Left:* The SQ mesh has been obtained by inverting the vertex planes of an A-net parametrization of a discrete Euclidean minimal surface in a sphere. Then all vertex spheres would pass through the center of the sphere of inversion and constitute a so-called *orthogonal s-net*. The vertex spheres of an orthogonal s-net are central spheres as pointed out in [Pellis et al. 2020]. We then grew the radius of the center point to an absolute sphere Ω while keeping s-net parameter curves orthogonal and the vertex spheres orthogonal to Ω. The result is a discrete central sphere congruence with spheres orthogonal to the absolute sphere Ω, hence a discrete minimal surface in hyperbolic space. All annuli forming the support structure are orthogonal to Ω. *Right:* We applied the adapted face size algorithm to a subdivided mesh of the SQ mesh on the left. The resulting ST mesh has been optimized for minimal intersection angles and face spheres being orthogonal to Ω. The latter optimization did not change its input much. We kept the supporting annuli in the image thin compared to the SQ mesh (right) not to cover too much of the faces.

Central spheres in a linear complex. The face spheres of ST meshes with support structure must lie in a *linear sphere complex* [Kilian et al. 2023]. There are three types of such linear complexes. (i) All its spheres are orthogonal to a real sphere Ω. (ii) All its spheres pass through a fixed point m. (iii) All its spheres are orthogonal to a sphere Ω with imaginary radius $R \in i\mathbb{R}$ (or equivalently, the spheres intersect the concentric real sphere Ω^r with radius $|R|$ in great circles; see Fig. 17 right).

We start with case (ii) where we are given a surface f with all its central spheres passing through a common point m. We apply an inversion ι in a sphere centered at m. Consequently, m is mapped to ∞ and all spheres of the complex become planes, hence, all central spheres of $\iota(f)$ are tangent planes. Surfaces whose central spheres are tangent planes are exactly the Euclidean minimal surfaces. Hence, the inverse images of minimal surfaces have central spheres through a fixed point (inversion center).

In the other two cases, the central spheres are actually planes in conformal models of non-Euclidean geometries based on the absolute spheres Ω. In case (i), the geometry is hyperbolic, and in case (iii) it is elliptic. The surfaces whose central spheres are in the linear complex are therefore minimal surfaces of hyperbolic geometry for type (i) and minimal surfaces of elliptic geometry of type (iii) (cf. [Blaschke 1929, p. 371]).

Recall that the central sphere is also the Meusnier sphere to the bisecting directions of the principal directions (whose normal curvature equals H). This leads to the following computation of such minimal surfaces based on a discrete model with principal symmetric and discrete orthogonal meshes. Principal symmetric meshes are characterized by spherical vertex stars, the spheres being discrete Meusnier spheres. By orthogonality of parameter lines they become central spheres (see [Pellis et al. 2020]). In addition we have to make sure that these vertex spheres lie in a linear complex. We will take advantage of these insights to obtain non-Euclidean minimal surfaces (Sec. 4): We start with an inverse image of a Euclidean minimal surface and gradually change the radius of Ω from 0 to the desired value R through optimization. These differential geometric properties do not only apply to ST but also to SQ meshes. We show examples in Figures 11, 17 and 18.

Surfaces with constant mean curvature. For a surface f with constant mean curvature $H \neq 0$ (CMC surface), the center surface c and second envelope $\bar{f}$ are offsets at distance $1/H$ and $2/H$, respectively. It is well known that c is also a CMC surface (see, e.g., [Bobenko and Suris 2008, p. 27]). As mentioned above, this implies that $\mathcal{L}$ is the common normal congruence of f as well as $\bar{f}$ and properties (a), (b) and (c) (cf. Sec. 2.5) are optimally fulfilled. Application of a Möbius transformation keeps properties (a) and (c), but one has to check whether (b) is within tolerance.

Congruences with simultaneous central spheres for both envelopes. Willmore surfaces are critical points of the Willmore energy. They are the Möbius geometric analogues to minimal surfaces of Euclidean, elliptic or hyperbolic geometry, and therefore called *Möbius-minimal surfaces* in the work of Blaschke [1929, pp. 371-377]. There, they arise as envelopes of those sphere congruences $\mathcal{S}$ which simultaneously are central spheres of both envelopes. The mapping $f \mapsto \bar{f}$ between envelopes is conformal. These double-central congruences are R-congruences only if the envelopes are isothermic surfaces, which happens exactly in the above mentioned cases of Euclidean and non-Euclidean minimal surfaces.

Unfortunately, general Willmore surfaces whose central spheres do not form an R-congruence, have everywhere imaginary torsal directions. More precisely, they are minimal lines, i.e., imaginary lines on the associated central spheres. This follows from the fact that the conformal map $f \mapsto \bar{f}$ is orientation reversing with respect to the contact spheres [Blaschke 1929, p. 383, probl. 4]. Therefore, it is not possible that corresponding tangents on $f, \bar{f}$ are coplanar with the connecting line L. As fixed lines of a rotation in the tangent plane of f (and $\bar{f}$) the torsal directions are minimal lines. Thus, the central sphere congruence of a general Willmore surface has no *real* parameterization such that the associated line congruence is torsal.

Surfaces without change in sign of H. Our computational approach uses the centers of spheres, and we initialize with the congruence of central spheres. Therefore, we cannot allow points with $H = 0$, i.e., central planes. Excluding the case of minimal surfaces ($H \equiv 0$), such points can form curves in negatively curved areas. Since the sign of H is not Möbius invariant, we are leaving here Möbius geometry.

In particular for architectural applications, considering surfaces without sign change of H is quite natural, since they appear as equilibrium shapes under gravity load. In their work on rapidly deployable structures of auxetic materials [Konakovic-Lukovic et al. 2018] took advantage of a sign constraint on H for deployment with balloons or gravity.

3 MESHES WITH ADAPTED FACE SIZE

Let us consider a given reference surface $\mathcal{R}$. The goal of this section is to generate a sphere mesh with large spherical panels in those areas of $\mathcal{R}$ that are approximately spherical already. For that we first generate an adaptive triangle mesh $\mathcal{M}$ with planar faces that has large faces in regions that can be approximated with large spherical patches. To obtain $\mathcal{M}$ we take a remeshing/decimation approach and assume that $\mathcal{R}$ is given as a dense triangle mesh.

Pliant remeshing. Let us assume we are given a function $g : \mathcal{R} \to \mathbb{R}^+$ on the reference surface that locally determines desired target edge lengths of an approximating triangle mesh. Then, for any triangle mesh with vertices on or near the reference surface we define the so-called *normalized length* of an edge e as

$$l(e) := |e|/g(\pi(e)), \tag{6}$$

where $\pi(e)$ denotes the projection of the edge midpoint onto $\mathcal{R}$. The goal is to reach a mesh with unit normalized edge length, i.e., $l(e) = 1$, in the metric (6). The normalized edge length drives the remeshing algorithm presented in Kobbelt et al. [2000] by working repeatedly through the following steps: (i) split all edges whose normalized edge length exceeds $4/3$, (ii) collapse all edges whose normalized edge length falls below $4/5$, (iii) perform edge flips to obtain vertex degree close to 6, (iv) perform Laplacian mesh smoothing. Repeating steps (i)-(iv) ten times yields good results. Here the function g itself is determined via so called influence zones.

Influence zones. To approximate a surface with a small number of spheres we compute a region U_i around a surface point v_i which is close within a given tolerance ε to the central sphere C_i at v_i (see Fig. 13). Starting from v_i we collect vertices v' around v_i in a breadth-first manner as long as the distance of v' to C_i is smaller than ε. The region U_i obtained in this way is roughly disk-shaped and we use its diameter as the value $g(v_i)$. The obtained values

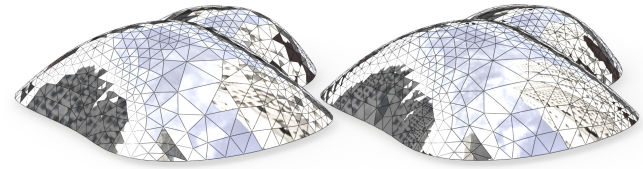

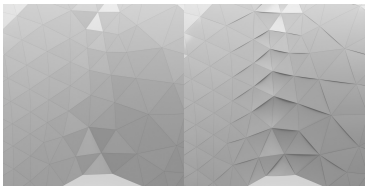

Fig. 12. Sphere meshes with adapted face sizes. We reduce the number of faces of a given mesh from about 2000 to 1346 faces. Both meshes have been optimized for minimal intersection angles. The difference is that the image on the *left* has additionally been optimized for edge-circles being as-orthogonal-as-possible to the reference surface $\mathcal{R}$. The edge-circles in the mesh on the *right* are generated by intersecting adjacent spheres with bisecting face planes resulting in small gaps appearing between faces, particularly in negatively curved areas (see close-ups). Those gaps are not problematic as long as they stay within fabrication tolerances. However, note that the sphere mesh on the *right* appears visually much smoother in positively curved areas. This is due to omitting the condition on edge-circles in orthogonal planes.

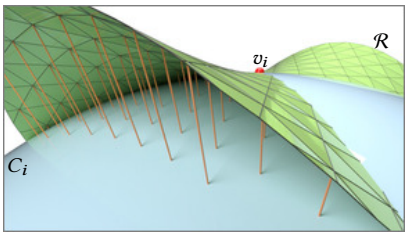

Fig. 13. Influence zone: We approximate the central sphere C_i (blue) at a vertex $v_i \in \mathcal{R}$ and determine the region where the distances of the vertices of a reference surface $\mathcal{R}$ are smaller than a given threshold.

at vertices of $\mathcal{R}$ are linearly interpolated across its triangles. To estimate C_i we use the jet-fit method [Cazals and Pouget 2005] to first find the osculating paraboloid whose mean curvature at the contact point v_i is the same as that of $\mathcal{R}$. Note that we can take any kind of 'locally optimal' sphere instead of C_i, cf. Fig. 9 and 16 where we have used local least-squares spheres that are orthogonal to a prescribed absolute sphere Ω (see Sec. 4).

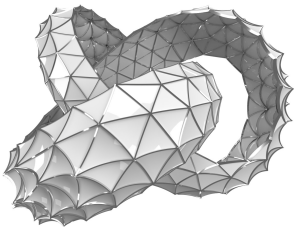

In the figure aside we experimented with different radii for the absolute sphere Ω' for the triangulation of Fig. 16 (top row). It can result in interesting shapes like this 'spiky' looking knot. Its face spheres are orthogonal to Ω' with large radius (larger than the radius of the optimal sphere Ω).

Angle-minimizing ST meshes. The curvature averaging nature of the central spheres makes them close to being angle minimizing among all sphere congruences which has already been pointed out by [Kilian et al. 2023]. Consequently, computing a new triangle mesh by adapting its face sizes to the values obtained from our influence zone estimation, the angle optimization of [Kilian et al. 2023] converges quickly to an angle minimizing sphere mesh when face spheres are initialized with central spheres. For examples we refer particularly to the meshes illustrated in Fig. 2, 12, 15, 11 (right).

4 ST MESHES WITH SUPPORT STRUCTURE

As pointed out by Kilian et al. [2023], an ST mesh can only have a support structure if all its node axes pass through a point m. The corresponding face spheres lie in a linear complex with base sphere Ω, with center m and radius R which can be real or imaginary, i.e, $R^2 \in \mathbb{R}$. A limit case is given if all node axes are parallel to a fixed line a, i.e., m is at infinity, and Ω is a plane orthogonal to a. Here, all face spheres have centers in Ω.

Approximation of a given surface by an ST mesh requires the computation of a good choice for Ω. In view of requirement (b), we first compute m and then R^2. The first step is also a contribution to the computation of a torsion free support structure of a triangle mesh that is realized with flat panels, since all node axes must pass through a point m and should be as orthogonal as possible to the reference surface.

Let the surface to be approximated be given as triangle mesh $\mathcal{M} = (V, F)$, where $v_i \in V$ are vertices, $f_i \in F$ are faces, with fixed orientation and normal vector field n_i. An absolute sphere Ω is defined by its center m and radius $R^2 \in \mathbb{R}$.

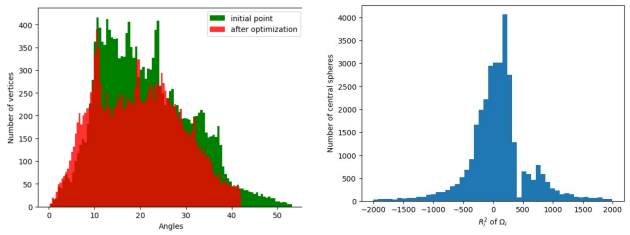

Fig. 14. Finding the absolute sphere Ω for the mesh in Fig. 9. The histogram (*left*) shows in green angles $\angle(v_i - m, n_i)$ for the initial guess of $m = m_0$ solving (7) and in red for m of the optimized absolute sphere. The histogram (*right*) shows the distribution of squared radii R_i^2 of central spheres.

Estimating the center m. An ST mesh has a practically useful support structure if the lines connecting m with vertices v_i have minimal angle $\alpha_i = \angle(v_i - m, n_i)$ with every normal n_i. For that we consider the following energy

$$E_{\text{center}} = \sum_{i\in|V|} (1 - \cos(\alpha_i)^2)^2 = \sum_{v_i\in V} \left(1 - \frac{\langle v_i - m, n_i\rangle^2}{\|v_i - m\|^2}\right)^2$$

and use the Levenberg-Marquardt algorithm [Marquardt 1963] to minimize it.

As initial choice for m we take the point m_0 that minimizes the sum of squared distances to the normal lines G_i at vertices v_i given by $G_i = v_i + tn_i$ with $t \in \mathbb{R}$. We denote by $Q_i \in \mathbb{R}^{3\times 3}$ a matrix such that $Q_i(v_i - m_0) = n_i \times (v_i - m_0)$ and consider the following energy

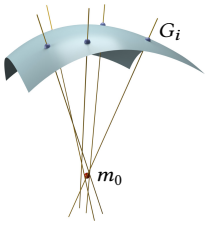

$$\sum\nolimits_{i\in|V|} \text{dist}(m_0, G_i)^2 = \sum\nolimits_{i\in|V|} \frac{1}{2}\|n_i \times (v_i - m_0)\|^2 \qquad (7)$$
$$= \frac{1}{2}\sum\nolimits_{i\in|V|} \|Q_i(v_i - m_0)\|^2 = \|Qm_0 - b\|^2,$$

where $Q = (Q_1, Q_2, \ldots)^T$, $b = (Q_1v_1, Q_2v_2 \ldots)^T$. We compute a least-squares solution by solving the corresponding normal equation $Q^TQm_0 = Q^Tb$. If the point m_0 is on the positive part with respect to the orientation of $\mathcal{M}$ we change the orientation.

Estimating the radius R. Now we need to find the radius R of the absolute sphere Ω. By choosing R, we obtain a unique linear complex of spheres which are orthogonal to Ω. Our face spheres S_i (panels) should locally approximate the given surface well. Thus, we try to find R such that spheres S_i are close to central spheres. For each central sphere C_i (center c_i, radius r_i) we compute the radius R_i^2 of a sphere Ω_i with center m that is orthogonal to C_i via $R_i^2 = \|m - c_i\|^2 - r_i^2$. We take for R^2 the mean over all R_i^2.

If m tends to be far away from the input surface, then the sphere Ω becomes very large and appears almost as a plane. Our algorithm detects that case and sets m at infinity. For that we first compute the direction a of node axes as the spherical barycenter of the Gauss image formed by the unit normal vectors at vertices of the given triangle mesh. We initialize this nonlinear problem with the barycenter and take any plane P_0 orthogonal to a as reference plane. The plane Ω lies at a distance d to P_0. Just as we compute the best radius of Ω, we now compute the best distance d. Each central sphere center has a distance d_i and we take the mean value.

ST meshes with support structure are illustrated in Fig. 9, 11 (right), 16. In Fig. 14 we show the histogram of R_i^2 for central spheres of the surface in Fig. 9.

5 APPROXIMATION WITH SQ MESHES

Our approximation of surfaces by SQ meshes takes as given reference surface a B-spline surface $f(u, v)$ with degree ≥ 5 in each of the parameters u, v. Our optimization strategy in this section falls into line with the rest of the paper except that we utilize the "smoothness" of the input surface to keep a smooth/exact representation of the sphere congruence throughout the first part of our optimization.

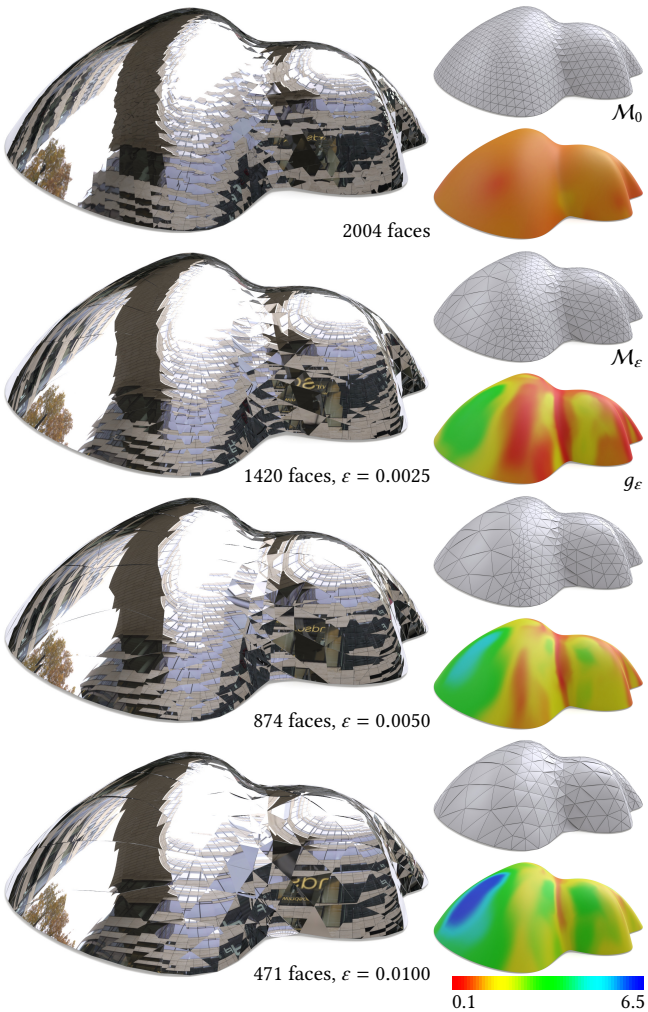

Fig. 15. *Top row, right column*: Initial triangulation $\mathcal{M}_0$ of the reference surface $\mathcal{R}$ and its edge lengths visualized as a color gradient. *Left column*: Corresponding angle minimizing ST mesh rendered with a reflective material. Successive rows show angle minimizing ST meshes, their triangulation $\mathcal{M}_\varepsilon$, and the corresponding size function g_ε for increasing values of ε.

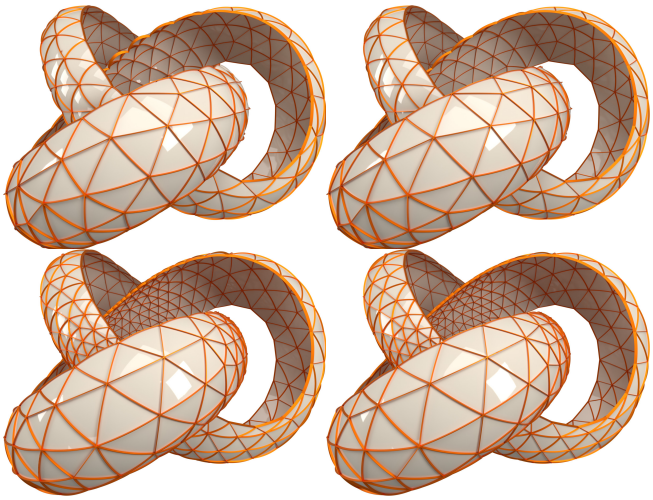

Fig. 16. ST mesh of a knot with support structure. *Top row*: Triangulation obtained by pliant remeshing using central spheres for the computation of influence zones. *Bottom row*: Instead of central spheres we use local least-squares spheres orthogonal to a prescribed absolute sphere Ω to determine influence zones. *Left column*: Panels obtained as spheres passing through the vertices of triangles and orthogonal to Ω. *Right column*: Taking the panels from the left we allow the radius R of Ω to change. Vertex coordinates of the mesh are fixed. We determine R by minimizing intersection angles of neighboring spheres such that face spheres remain orthogonal to the varying absolute sphere Ω. The smoothest solution is on the *bottom right*.

The sphere congruence uses a radius function which we represent in B-spline form

$$r(u,v) = \sum_{kl} N_k^m(u) N_l^n(v) r_{kl} \tag{8}$$

over the same spline basis as the given reference surface f. Our sphere congruence $\mathcal{S}$ is now given by radii $r(u,v)$ and centers $c(u,v)$

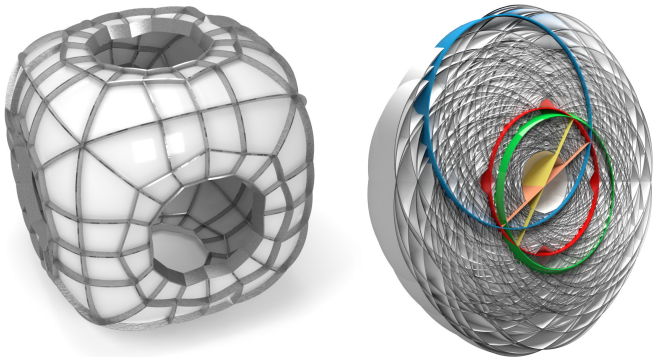

Fig. 17. Polyhedral quad surface in elliptic space. It is similar to Fig. 11 except that the absolute sphere Ω is not real but has a negative squared radius R. Its concentric real sphere Ω^r with radius $|R|$ is illustrated in red (*right*). All face spheres intersect Ω^r along a great circle, i.e., the intersection circles lie in planes through the center of Ω^r. We emphasized two spheres (green, blue) and their intersection with Ω^r.

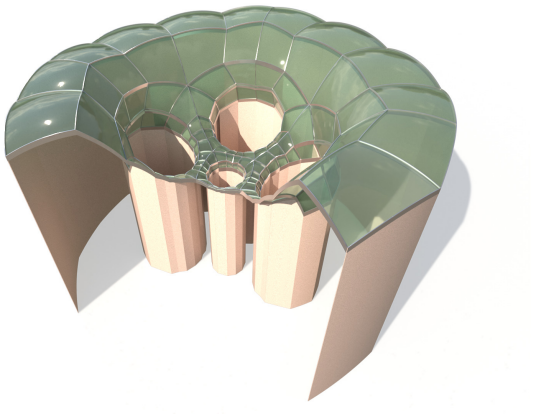

Fig. 18. A "roof" modeled as SQ mesh with vertical support structure. The face spheres are orthogonal to a horizontal plane. The support structure is therefore contained in vertical planes some of them realized as "walls". Geometrically, the roof itself is a polyhedral surface in the Poincare half space model of hyperbolic geometry $\mathbb{H}^3$. This SQ mesh is an inverse image of the SQ mesh in Figure 11.

from Equation (1). The center surface is a smooth surface but in general not a B-spline surface as the normalization in the normal vector field $n(u,v)$ involves a square root.

We initialize our sphere congruence with a B-spline approximation of the central congruence. To that end we sample the smooth surface f along a grid G. For each $(u_i, v_j) \in G$ we compute the central sphere radius r_{ij} at $f(u_i, v_j)$ and approximate these data by a B-spline function $r(u,v)$ as in Equation (8).

From that, the lines $L(u,v)$ of the associated line congruence $\mathcal{L}$ at each point (u,v) are found via the equations described in Section 2.1: $L \parallel c_u \times c_v$ and $L(u,v)$ pass through $f(u,v)$.

Our approach is to first optimize the sphere congruence in such a way that its associated line congruence admits two real torsal directions and fulfills desired requirements (as listed in Sec. 2.5). We compute the torsal directions on each face of the grid G and define a cross field over a quad mesh in this way. A remeshing algorithm is used to obtain a quad mesh that follows the torsal cross field. This mesh is already close to our solution but whose precision is improved in a final optimization step (Sec. 5.2).

5.1 Congruence optimization

With our first optimization step we find a sphere congruence $\mathcal{S}$ such that we have a good approximation of the reference surface (Sec. 2.5 prop. (a)) and with a good support structure (properties (b) and (c)). As described in Sec. 2, central spheres are good approximations. However, depending on the reference surface f, the central sphere congruence can induce an associated line congruence where the lines can be nearly tangential to the surface f, or the torsal directions could be very close (almost parallel) resulting in a bad support structure. Even worse, the torsal directions could be imaginary. Thus, the aim of this first optimization is to determine the control values r_{kl} of the B-spline function $r(u,v)$ such that the associated line congruence lies within our prescribed angle threshold θ. We take the

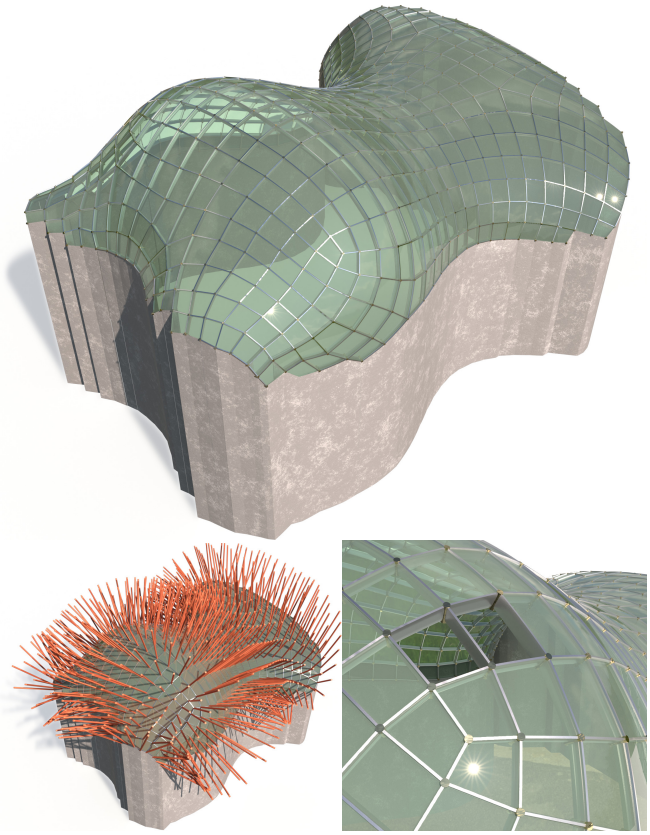

Fig. 19. A "roof" as SQ mesh with support structure approximating a given reference surface with a sphere congruence whose associated line congruence $\mathcal{L}$ has real torsal directions fulfilling requirements (b) and (c) from Sec. 2.5. The lines of $\mathcal{L}$ are therefore well suited for node axes (*bottom left*) of the support structure. The whole process of constructing this SQ mesh which mainly splits into two optimization steps is described in Sec. 5.

central sphere congruence as an initial guess for that optimization step. Variables in our optimization are the control values r_{ij} and direction vectors l_{ij} of the lines of the congruence $\mathcal{L}$ at parameter values (u_i, v_j). We constrain l_{ij} to have unit lengths.

We proceed in two steps. First, we ensure that l_{ij} stays in the associated line congruence by orthogonality to c_u and c_v, at the corresponding grid points (u_i, v_j)

$$E_{\mathrm{LC}} = \sum\nolimits_{i,j\in G} \langle l_{ij}, c_{ij,u}\rangle^2 + \langle l_{ij}, c_{ij,v}\rangle^2,$$

where the comma at the subscript $c_{ij,u}$ indicates the derivative $\frac{\partial c}{\partial u}$ evaluated at (u_i, v_j).

Good angles of l_{ij} to the surface f, i.e., $\langle l_{ij}, n_{ij}\rangle \geq \theta$ (property (b)) are expressed with dummy variables μ_{ij} by the following objective function,

$$E_{\mathrm{LC_{orth}}} = \sum\nolimits_{i,j\in G} (\langle l_{ij}, n_{ij}\rangle^2 - \theta^2 - \mu_{ij}^2)^2.$$

The square in the first term is used to avoid problems with the directions of the lines. If some lines are flipped with respect to the normal of the surface, we flip them back at the end of the first step.

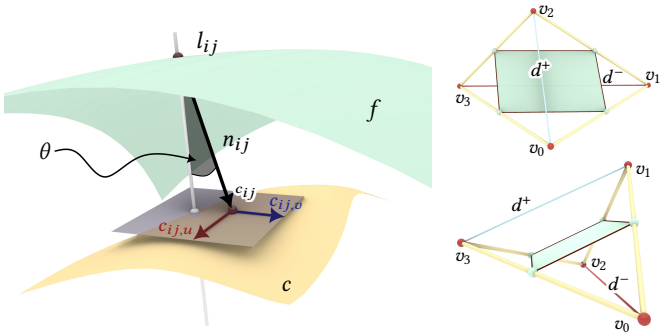

Fig. 20. *Left*: Illustration of the line congruence setup for the optimization. *Right*: Notation of the elements involved in checkerboard patterns.

In a second step, we focus on suitable torsal directions. Here we want the intersection angle of the torsal planes not to deviate too much from $\pi/2$. For this, we take advantage of the approximation quality of the first order derivatives from so-called checkerboard pattern meshes (see [Jiang et al. 2021] and Fig. 20 right). Let us consider a quadrilateral q corresponding to $(v_0, v_1, v_2, v_3) \in G$. The midpoints of the four edges of q form a parallelogram b. Its plane is known to be a discrete version of a tangent plane. The diagonal vectors $d^+ = v_2 - v_0$ and $d^- = v_1 - v_3$ approximate well the tangent vectors $f_u \pm f_v$ at the center of q.

All our parametrizations $f, \bar{f}, c, l$ are related by the same parameters u, v. Hence, tangent vectors in the tangent spaces spanned by the partial derivatives correspond by the same linear combinations. For example, the tangent vector $\mu_0 f_u + \mu_1 f_v$ corresponds to the tangent vector $\mu_0 l_u + \mu_1 l_v$, etc.

In analogy to the discrete tangent vectors d^+, d^-, we can approximate derivatives of the line congruence as $l^+ = l_2 - l_0$ and $l^- = l_1 - l_3$. Thus, we can parametrize a vector direction on each quad b as

$$t = \mu_0 d^+ + \mu_1 d^- \quad \text{which implies that} \quad l_t = \mu_0 l^+ + \mu_1 l^-.$$

The torsal directions should satisfy the planarity condition of the plane spanned by $\{l_t, t, l_c\}$, where l_c is the line of the congruence $\mathcal{L}$ at the barycenter of q. In our optimization, we incorporate this condition by the energy

$$E_{\mathrm{torsal}} = \sum\nolimits_{q\in Q} \langle \frac{l_t}{\|l_t\|}, n_q^*\rangle^2 + \langle \frac{l_c}{\|l_c\|}, n_q^*\rangle^2 + \langle t, n_q^*\rangle^2.$$

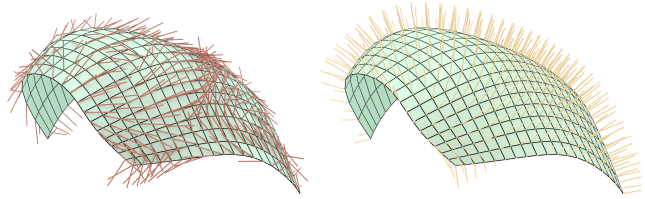

Fig. 21. *Left*: Associated line congruence of the central sphere congruence corresponding to the reference surface. *Right*: Optimized line congruence with $\theta = 15°$ (=angle threshold between surface normal and line of the line congruence) and $\alpha = 60°$ (=angle threshold between torsal planes).

Here, n_q^* are auxiliary variables that represent the normal of the plane spanned by $\{l_t, t, l_c\}$. We add constraints $\|t\| = \|n_q^*\| = 1$. We formulate E_{torsal} for both torsal directions, $t = t_1$ and $t = t_2$. This allows us to formulate the angle constraints on torsal directions as

$$E_{\text{angle}} = \sum_{q \in Q} (\langle n_{q,\,t_1}^*, n_{q,\,t_2}^* \rangle^2 - \cos^2 \alpha + v_q^2)^2,$$

where v_q are dummy variables to represent the inequalities. α is the threshold for the angle between the torsal planes. We also add a Laplacian fairness to the line congruence in this optimization.

Implementation details. The variables in this Levenberg-Marquardt optimization are

- l_{ij} line congruence directions,
- r_{ij} control values in the B-spline representation for radii $r(u, v)$,
- μ_0, μ_1 for the direction of the torsal directions t; one pair per each torsal direction,
- n_q^* for the normal vector for each torsal plane.

During the optimization, the torsal directions, together with the plane normal vectors n_q^*, are recomputed after a defined number of steps. This prevents the optimization from getting stuck with degenerated torsal directions and has proven to yield faster convergence. In the last steps of the optimization, we set the weights $w_{\text{angle}} = w_{\text{fair}} = 0$ to improve the correctness of the torsal directions.

The optimization algorithm that we use [Tang et al. 2014] uses a regularizing energy E_{reg} which prevents abrupt changes in the variables. We utilize this energy for our variables n_{q,t_i}^* controlling planarity of the torsal planes.

Putting together all the energies above and multiplying them with appropriate weights yields the total energy:

$$E = w_{\text{LC}} E_{\text{LC}} + w_{E_{\text{LC}_{\text{orth}}}} E_{E_{\text{LC}_{\text{orth}}}} + w_{\text{torsal}} E_{\text{torsal}} + w_{\text{angle}} E_{\text{angle}} + w_{\text{fair}} E_{\text{fair}} + w_{\text{reg}} E_{\text{reg}}. \quad (9)$$

The weights for the illustrated examples can be found in Tables 1 and 2 in Section 6.

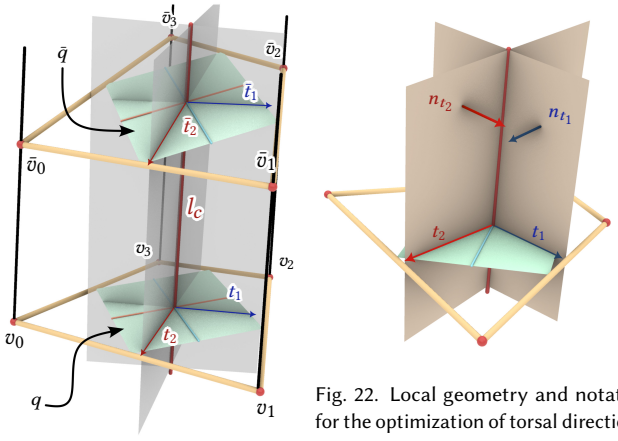

Fig. 22. Local geometry and notation for the optimization of torsal directions.

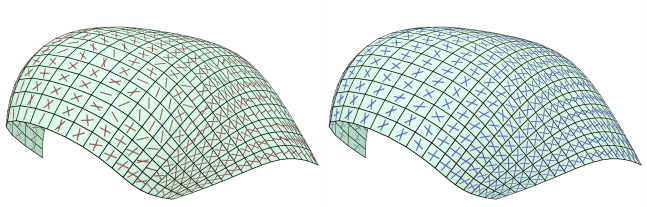

Fig. 23. *Left*: Torsal directions computed with the induced line congruence of the central sphere congruence without optimization. *Right*: Optimized torsal directions with $\theta = 15°$ (=angle threshold between surface normal and line of the line congruence) and $\alpha = 45°$ (=angle threshold between torsal planes).

5.2 Quad remeshing with torsal directions

We perform a quad remeshing by following the torsal directions computed in Section 5.1. We used Rhino plugin implementations of IGL Anisotropic remeshing described in [Panozzo et al. 2014] and LibQEx from [Ebke et al. 2013] to obtain a quad mesh being aligned with the torsal directions. The edges of the resulting mesh are no longer exactly the discrete torsal directions for the optimized line congruence. Moreover the vertices are not exactly contained in the given B-spline surface and we need to find the spheres per face. This is done in the following final optimization step.

The resulting quad mesh from above may exhibit some zigzag behavior which we eliminate by letting the mesh glide over the reference surface while enforcing fairness of the parameter lines. In this way we obtain a fair quad mesh Q'.

By a simple least squares method we now compute for each vertex $q_{ij} \in Q'$ the corresponding parameters (u_i, v_j) within the parameter domain of the given B-spline reference surface.

Our final task is to convert Q' into our desired SQ mesh. For that, we first convert Q' into a discrete sphere congruence $\mathcal{S}^*$ with centers $c_{ij} = q_{ij} + r_{ij} n_{ij}$, where $r_{ij} = r(u_i, v_j)$. From $\mathcal{S}^*$ we compute a discrete sphere congruence $\mathcal{S}$ with a sphere for each face $q \in Q'$ by averaging the centers and the radii (see Fig. 24 left). Now we take $\mathcal{S}$ as an input for a final post optimization with the goal that *(i)* the spheres of $\mathcal{S}$ pass through Q', *(ii)* neighboring node axes are co-planar (discrete torsal planes for the existence of a support structure), *(iii)* proximity to the reference surface, and *(iv)* fairness of the resulting SQ mesh.

For the *sphere fitting (i)*, we use the same approach as in [Kilian et al. 2023] where they represented the spheres with implicit equations in the form $\psi(\mathbf{x}) := A\mathbf{x}^2 - \langle B, \mathbf{x} \rangle + C = 0$, where $B = (B_1, B_2, B_3) \in \mathbb{R}^3$, $A, C \in \mathbb{R}$, and where $\langle \cdot, \cdot \rangle$ denotes the Euclidean scalar product. Following [Kilian et al. 2023] the energy term used for the sphere fitting reads

$$E_{\text{sphere}} = \sum_{f \in F} \sum_{q_i \in f} \psi^2(q_i) \quad \text{and} \quad E_{\text{unit}} = \sum_{f \in F} \varphi^2(f),$$

where $\varphi(f) := B_f^T B_f - 4 A_f C_f - 1$ is used to normalize the coefficients of the sphere equation and prevents the coefficients from vanishing.

To ensure the existence of a torsion free node at each vertex $q \in Q'$ we require planar faces in the mesh of centers c_{ij}. Per each non-boundary vertex $q \in Q'$ there are four spheres intersecting at q. The four corresponding centers for a face c_q of the mesh of centers.

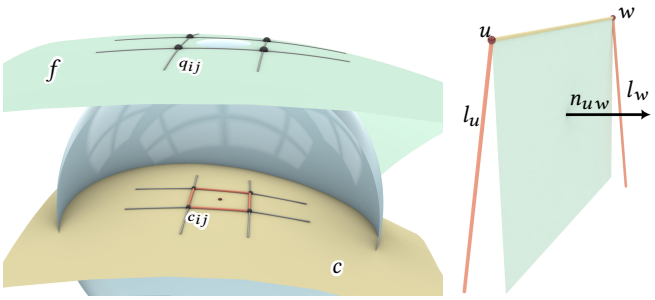

Fig. 24. *Left:* Notation in the computation of the initial guess for the sphere congruence corresponding to Q'. The sphere corresponding to vertex $q_{ij} \in Q'$ has its center c_{ij} in the surface c. *Right*: Notation for the planarity energy of the discrete torsal planes. The edge uw and the two torsal lines l_u, l_v must become planar in the optimization.

To obtain planarity of c_q we minimize the squared scalar product of edge vectors $c_i - c_j$ with an auxiliary normal vector n_{c_q} per face. We denote the scalar product by $\psi(c_i c_j) := \langle c_i - c_j, n_{c_q} \rangle$. We initialize n_{c_q} with the direction of our optimized line congruence. Thus, the energy term for the existence of a support structure reads

$$E_{\text{supp}} = \sum\nolimits_{c_q} \sum\nolimits_{c_i c_j \in c_q} \psi^2(c_i c_j),$$

with the constraint $\|n_{c_q}\| = 1$.

To ensure the existence of a *support structure (ii)* we optimize for planarity of neighboring node axes l_u, l_w and each edge uw. This energy term uses an auxiliary variable n_{uw} representing the normal vector of the plane:

$$E_{\text{torsal plane}} = \sum_{uw \in \text{edges}} \langle l_u, n_{uw} \rangle^2 + \langle l_w, n_{uw} \rangle^2 + \langle \frac{w-u}{\|w-u\|}, n_{uw} \rangle^2,$$

with the constraint $\|n_{uw}\| = 1$. We initialize the normal vectors n_{uw} of the planes of the support structures as the normalized cross product of $u - w$ with $l_u + l_w$, the average of the corresponding line vectors of the line congruence; see Fig. 24 (right).

We include a *proximity* term *(iii)* for the closeness of Q' to the reference surface f. Following [Tang et al. 2014] we express the proximity in terms of distance to the corresponding tangent plane and distance to the corresponding point on the reference surface:

$$E_{\text{prox}} = \sum\nolimits_{v \in Q'} \langle v - v_f, n_f \rangle^2 + \epsilon (v - v_f)^2,$$

where v_f is the closest point of v on the reference surface. n_f is the unit normal vector of f at v_f. We use a small value of ϵ to control the closeness to the reference surface. The same is done for the surface of the sphere centers.

Finally, we include some *regularization* energies *(iv)*. These include fairness terms for quad meshes as described in [Tang et al. 2014] and dampening terms for the change of variables. The total energy used for computing the final sphere congruence is

$$\begin{aligned} E = {} & w_{\text{prox}_f} E_{\text{prox}_f} + w_{\text{prox}_C} E_{\text{prox}_C} + w_{\text{torsal plane}} E_{\text{torsal plane}} \\ & + w_{\text{sphere}} E_{\text{sphere}} + w_{\text{unit}} E_{\text{unit}} + w_{\text{supp}} E_{\text{supp}} + w_{\text{fair}} E_{\text{fair}} + w_{\text{reg}} E_{\text{reg}}. \end{aligned} \quad (10)$$

The weights for the examples can be found in Table 3 (Sec. 6).

Implementation details. The variables of our optimization are

- A, B, C values determining the sphere per face of Q',
- the vertices $v \in Q'$,
- the normals n_{uw} of the discrete torsal planes per edge uw,
- the normal vectors n_{c_q} for each face of the sphere center mesh.

We perform a 'warm-up' optimization of a few steps, where the only variables are the spheres. We optimize only for sphericity and a small value for the support structure; this allows us to have a closer initial guess before starting to allow the movement of the vertices Q' during the optimization. Then, we perform the full optimization with the rest of the variables and energies mentioned before.

6 RESULTS AND DISCUSSION

We have constructed sphere meshes by approximating given reference surfaces in three different ways: (i) through generating ST meshes by adapting face sizes but without support structure (Sec. 3), (ii) by approximating with ST meshes with support structure (Sec. 4), and (iii) by approximating with SQ meshes with support structure (Sec. 5).

6.1 ST mesh approximation

Adapted face sizes. Method (i) generically generates the smoothest results since we do not require that the edge circles around each vertex lie in planes that meet in an axis. We experimented with the top of the so called "Lilium tower" (Fig. 2) and the "Botanic garden" surface. Additional to intersection angle minimization we compare with an additional trade-off goal, namely with "nice" intersection circles of neighboring faces (Fig. 12 left). The smoother mesh is obtained without that goal but here we must cut face spheres using bisecting face planes resulting in small gaps (Fig. 12 right). Furthermore, we experimented with the same surface by reducing the number of faces in Figure 15. Clearly, the smoothness of positively curved areas is less effected under the reduction of the number of faces than negatively curved areas. For the knot surface in Figure 16 we have used different functions g to determine the desired edge lengths: in the top row g measures the size of the local region where the central sphere does not deviate from the surface within a given threshold, and in the bottom row the spheres are orthogonal to an estimated well suited absolute sphere Ω. We ran another round of intersection angle minimization on the meshes on the right hand side where the radius of Ω was treated as a variable. Thus the meshes on the right are a bit smoother.

Support structure. With method (ii) we generate ST meshes with support structure which implies that all face spheres must be orthogonal to an absolute sphere Ω with radius R (which can be real ($R > 0$), imaginary ($R^2 < 0$) or a point ($R = 0$)). All node axes must pass through a common point, the center of Ω (cf. Fig. 9). Every such ST mesh with a real absolute sphere Ω comes with a second ST mesh obtained by inversion in Ω (Fig. 10). If the central spheres are orthogonal to an absolute sphere we have a minimal surface in the respective non-Euclidean geometry: in hyperbolic space ($R > 0$) in Figure 11 and in elliptic space ($R^2 < 0$) in Figure 17. Applying a Möbius transformation which maps the real absolute sphere to a plane yields a support structure with node axes orthogonal to

that plane (Fig. 18). All four surfaces in Figure 16 are ST meshes with support structure (with a real absolute sphere Ω that is not illustrated in the Figure). These ST meshes are therefore polyhedral surfaces in a hyperbolic space. In applications one could play with "building tolerances" and generate ST meshes with more than one corresponding absolute sphere as illustrated by Figure 1.

6.2 SQ mesh approximation

Method (iii) yields SQ meshes with support structure by generating sphere congruences whose associated line congruences have suitable developable surfaces along their torsal directions. In a first optimization step we obtain a suitable line congruence (Fig. 21) corresponding to a given reference surface. After computing the tangential vector field of torsal directions and optimizing it for fairness, we integrate it to a quad mesh (Fig. 23). This quad mesh is a good initial guess for a final optimization step which produces the final result of an SQ mesh with support structure (Fig. 19, 25).

Parameters and timings. We provided details on the variables in our optimizations in the sections where they appear. Here we collect the tables with the bookkeeping (number of elements, weights, default values, residuals, etc.) of our illustrated examples. Residuals are normalized by the number of terms.

Table 1. Associated line congruence optimization. We set $w_{\text{LC}} = 1$ as default value. The times were measured for a Python implementation of our algorithm on a Macbook Pro with an M1 8-core CPU, 8-core GPU, and 16-core Neural Engine.

Fig	|V|	|F|	θ	α	$w_{\text{LC}_{\text{Orth}}}$	it	time (s/it)	res
23,21	400	361	15°	45°	2	100	0.02	$1.17E{-}21$
25	400	841	25°	45°	2	40	0.04	$2.16E{-}18$
19	400	361	15°	45°	0.5	90	0.12	$5.72E{-}22$

Table 2. Torsal directions optimization. The default values are $w_{\text{LC}} = 1$, $w_{\text{LC}_{\text{Orth}}} = 0.01$, $w_{\text{torsal}} = 1$, $w_{\text{angle}} = 2$, $w_{\text{Fair}} = 0.1$, $w_{\text{reg}} = 0.05$. Empty entries in the table correspond to the default values. The *recomputation steps* (RS) specify the number of steps to recompute the torsal directions. The residuals in this table exclude the contribution of regularizers.

Fig	|V|	|F|	θ	α	w_{torsal}	w_{angle}	w_{Fair}	it	RS	time s/it	res
23,21	400	361	15°	60°	.5	2		100	10	.47	$9.43E{-}5$
25	400	841	25°	45°				100	10	2.22	$7.55E{-}6$
19	400	361	15°	45°			.5	100	25	.529	$1.53E{-}5$

6.3 Limitations

ST meshes with support structure possess limited freedom for approximation due to the strong geometric constraints. Our method for approximation with SQ meshes with support structure is limited to shapes without sign change in mean curvature. It occurs since we start with the central sphere congruence, i.e., the best fitting spheres, and optimize until constraints (b) and (c) from Sec. 2.5 are fulfilled. An approach where one starts with constant sphere radii (there (b) and (c) are fulfilled) and optimizes for a better fitting error gives rise to another type of curvature restriction (see the Shex mesh approximation in [Kilian et al. 2023] where the support structure always exists). We did not address Shex meshes, but the present congruence optimization without considering torsal directions is suitable for this application as well. The same holds for all other types of sphere meshes without support structure.

Table 3. Residuals and weights of sphere congruence optimization. The default weighs in the energy (10) are $w_{\text{torsal plane}} = 0.01$, $w_{\text{unit}} = 10$, $w_{\text{reg}_v=0.04}$, $w_{\text{reg}_n} = 0.05$. Here, $|\tilde{F}|$ is the number of faces after remeshing. The residuals in this table consider only the contributions from E_{sphere}, E_{supp}, $E_{\text{torsal plane}}$ and E_{prox}.

Fig	$\lvert\tilde{F}\rvert$	w_{prox_f}	w_{prox_c}	w_{fair}	$w_{\text{sph.}}$	w_{supp}	it	time (s/it)	res
23,21	237	0.2	0.1	0.2	2	0.5	200	0.49	$1.98E{-}6$
25	739	0.2	0.05	0.1	2	0.1	200	0.82	$4.54E{-}6$
19	500	0.1	0.01	2	0.5	0.01	200	0.93	$1.88E{-}6$

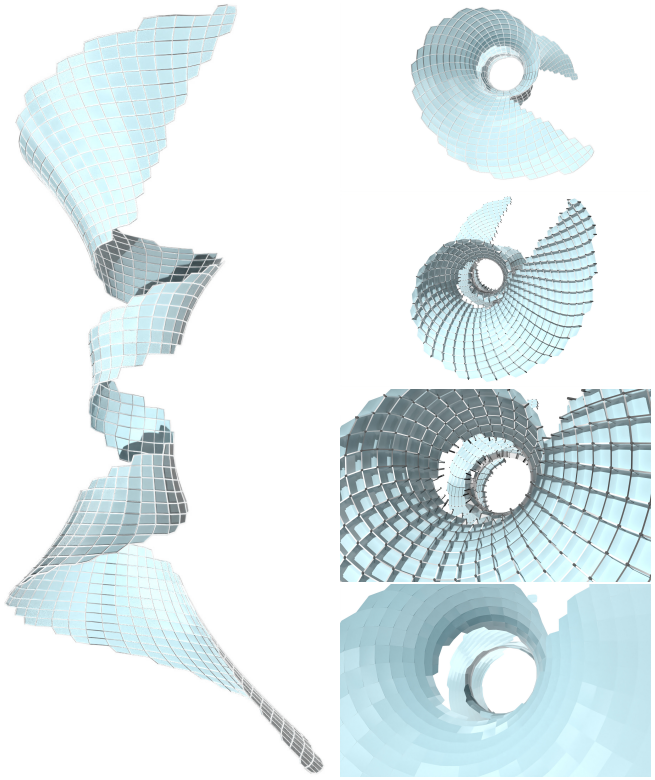

Fig. 25. *Left*: SQ mesh on a spiraling surface. *Right from top to bottom*: Surface with edges; surface with support structure; close up of support structure; close up to panels.

6.4 Future work

SQ mesh layout for architectural applications may also consider structural properties. While we aimed at high local approximation quality, this may actually not be desired and non-smoothness could be a design intent (cf. the inset in Sec. 3 in connection with influence zones). One may also explore applications beyond architecture, e.g., for cell packing structures such as the one in Fig. 8. Finally, we point to interesting aspects that arise when replacing Möbius geometry by sphere geometry of Laguerre or Lie.

ACKNOWLEDGMENTS

The authors gratefully acknowledge the support by the SFB-Transregio "Discretization in Geometry and Dynamics" through grant I 4868 of the Austrian Science Fund (FWF) as well as by project F77 (SFB "Advanced Computational Design") and by KAUST baseline funding. Furthermore, the authors would like to thank Hui Wang and Victor Ceballos Inza for sharing code segments and the anonymous reviewers for their valuable comments.

REFERENCES

Nina Amenta, Sunghee Choi, and Ravi Krishna Kolluri. 2001. The power crust, unions of balls, and the medial axis transform. *Comput. Geom. Theory Appl.* 19, 2–3 (jul 2001), 127–153.

Wilhelm Blaschke. 1929. *Vorlesungen über Differentialgeometrie und geometrische Grundlagen von Einsteins Relativitätstheorie. Band III. Differentialgeometrie der Kreise und Kugeln.* Springer, Berlin.

Wilhelm Blaschke. 1930. *Vorlesungen über Differentialgeometrie und geometrische Grundlagen von Einsteins Relativitätstheorie. Band I. Elementare Differentialgeometrie.* Springer, Berlin.

Alexander I. Bobenko and Peter Schröder. 2005. Discrete Willmore Flow. In *Proc. Eurographics Symposium on Geometry Processing*. Eurographics Assoc., 101–110.

Alexander I. Bobenko and Yuri B. Suris. 2006. Isothermic surfaces in sphere geometries as Moutard nets. *Proceedings of The Royal Society A Mathematical Physical and Engineering Sciences* 463 (2006), 3171–3193.

Alexander I. Bobenko and Yury B. Suris. 2007. On organizing principles of discrete differential geometry. Geometry of spheres. *Russian Mathematical Surveys* 62, 1 (2007), 1–43.

Alexander I. Bobenko and Yuri B. Suris. 2008. *Discrete differential geometry. Integrable structure.* Graduate Studies in Mathematics, Vol. 98. American Mathematical Society.

Peter B. Canham. 1970. The minimum energy of bending as a possible explanation of the biconcave shape of the human red blood cell. *Journal of theoretical biology* 26 1 (1970), 61–81.

Frederic Cazals and Marc Pouget. 2005. Estimating differential quantities using polynomial fitting of osculating jets. *Computer Aided Geometric Design* 22, 2 (2005), 121–146.

Ho-Lun Cheng and Xinwei Shi. 2005. Quality Mesh Generation for Molecular Skin Surfaces Using Restricted Union of Balls. In *16th IEEE Visualization Conference, Proceedings*. IEEE Computer Society, 399–405.

Ho-Lun Cheng, Tamal K. Dey, Herbert Edelsbrunner, and John Sullivan. 2001. Dynamic Skin Triangulation. *Discrete Comput. Geom.* 25, 4 (2001), 525–568.

Keenan Crane, Ulrich Pinkall, and Peter Schröder. 2013. Robust Fairing via Conformal Curvature Flow. *ACM Trans. Graph.* 32 (2013). Issue 4.

Manfredo do Carmo. 1976. *Differential Geometry of Curves and Surfaces.* Prentice-Hall.

Marc Droske and Martin Rumpf. 2004. A level set formulation for Willmore flow. *Interfaces and Free Boundaries* 6 (2004), 361–378.

Hans-Christian Ebke, David Bommes, Marcel Campen, and Leif Kobbelt. 2013. QEx: Robust quad mesh extraction. *ACM Trans. Graph.* 32, 6 (2013), 1–10.

Herbert Edelsbrunner. 1993. The Union of Balls and Its Dual Shape. In *Proceedings of the Ninth Annual Symposium on Computational Geometry (SCG '93)*. Association for Computing Machinery, 218–231.

Herbert Edelsbrunner. 1999. Deformable smooth surface design. *Discrete Comput. Geom.* 21 (1999), 87–115.

Gershon Elber, Gill Barequet, and Myung-Soo Kim. 1999. Bisectors and alpha-Sectors of Rational Varieties. In *Geometric Modelling*. Springer-Verlag, Berlin, Heidelberg, 73–88.

Gershon Elber and Myung-Soo Kim. 2000. A computational model for nonrational bisector surfaces: curve-surface and surface-surface bisectors. In *Proceedings Geometric Modeling and Processing 2000. Theory and Applications*. 364–372.

Evan Anthony Evans. 1974. Bending resistance and chemically induced moments in membrane bilayers. *Biophysical journal* 14 (1974), 923–931.

Stephen William Hawking. 1968. Gravitational radiation in an expanding universe. *J. Math. Phys.* 9 (1968), 598–604.

Udo Hertrich-Jeromin. 2003. *Introduction to Möbius Differential Geometry.* Cambridge University Press.

Elias Jadon, Bernhard Thomaszewski, Aleksandra Anna Apolinarska, and Roi Poranne. 2022. Continuous Deformation Based Panelization for Design Rationalization. *ACM Trans. Graph.*, Article 44 (2022), 8 pages.

Caigui Jiang, Hui Wang, Victor Ceballos Inza, Felix Dellinger, Florian Rist, Johannes Wallner, and Helmut Pottmann. 2021. Using isometries for computational design and fabrication. *ACM Trans. Graph.* 40, 4 (2021), 42:1–42:12. Proc. SIGGRAPH.

Martin Kilian, Anthony Cisneros Ramos, Christian Müller, and Helmut Pottmann. 2023. Meshes with spherical faces. *ACM Trans. Graph.* 42, 6 (2023), 177:1–177:19.

Felix Knöppel, Ulrich Pinkall, Peter Schröder, and Yousuf Soliman. 2023. Rolling spheres and the Willmore energy. arXiv:math.DG/2311.02241

Leif P. Kobbelt, Thilo Bareuther, and Hans-Peter Seidel. 2000. Multiresolution Shape Deformations for Meshes with Dynamic Vertex Connectivity. *Computer Graphics Forum* 19, 3 (2000), 249–260.

Thomas Koerber. 2020. The Area Preserving Willmore Flow and Local Maximizers of the Hawking Mass in Asymptotically Schwarzschild Manifolds. *The Journal of Geometric Analysis* 31 (2020), 3455 – 3497.

Mina Konakovic-Lukovic, Julian Panetta, Keenan Crane, and Mark Pauly. 2018. Rapid deployment of curved surfaces via programmable auxetics. *ACM Trans. Graph.* 37 (2018), 1 – 13.

Donald W. Marquardt. 1963. An Algorithm for Least-Squares Estimation of Nonlinear Parameters. *J. Soc. Indust. Appl. Math.* 11, 2 (1963), 431–441.

Daniele Panozzo, Enrico Puppo, Marco Tarini, and Olga Sorkine-Hornung. 2014. Frame fields: anisotropic and non-orthogonal cross fields. *ACM Trans. Graph.* 33, 4, Article 134 (2014), 11 pages.

Davide Pellis, Hui Wang, Martin Kilian, Florian Rist, Helmut Pottmann, and Christian Müller. 2020. Principal symmetric meshes. *ACM Trans. Graph.* 39, 4 (2020), 127:1–127:17. Proc. SIGGRAPH.

Martin Peternell. 2000. Geometric Properties of Bisector Surfaces. *Graph. Model.* 62 (2000), 202–236.

Helmut Pottmann, Caigui Jiang, Mathias Höbinger, Jun Wang, Philippe Bompas, and Johannes Wallner. 2015. Cell packing structures. *Computer-Aided Design* 60 (2015), 70–83. Special issue on Material Ecology.

Helmut Pottmann and Martin Peternell. 2000. Envelopes – Computational Theory and Applications. In *Spring Conference on Computer Graphics 2000*, B. Falcidieno (Ed.). Comenius University, Bratislava, 3–23. Proceedings of the conference in Budmerice, May 3-6, 2000.

Helmut Pottmann and Johannes Wallner. 2001. *Computational Line Geometry.* Springer.

Thilo Rörig and Gudrun Szewieczek. 2021. The Ribaucour families of discrete R-congruences. *Geom. Dedicata* 214 (2021), 251–275.

Kaleem Siddiqi and Stephen M. Pizer. 2008. Medial Representations: Mathematics, Algorithms and Applications *(Computational Imaging and Vision)*, Vol. 37. Springer.

Yousuf Soliman, Albert Chern, Olga Diamanti, Felix Knöppel, Ulrich Pinkall, and Peter Schröder. 2021. Constrained Willmore Surfaces. *ACM Trans. Graph.* 40, 4, Article 112 (2021), 17 pages.

Svetlana Stolpner, Paul Kry, and Kaleem Siddiqi. 2012. Medial Spheres for Shape Approximation. *IEEE Transactions on Pattern Analysis and Machine Intelligence* 34, 6 (2012), 1234–1240.

Feng Sun, Yi-King Choi, Yizhou Yu, and Wenping Wang. 2013. Medial Meshes for Volume Approximation. *ArXiv* abs/1308.3917 (2013).

Chengcheng Tang, Xiang Sun, Alexandra Gomes, Johannes Wallner, and Helmut Pottmann. 2014. Form-finding with Polyhedral Meshes Made Simple. *ACM Trans. Graph.* 33, 4 (2014), 70:1–70:9.

Jean-Marc Thiery, Emilie Guy, and Tamy Boubekeur. 2013. Sphere-Meshes: Shape Approximation using Spherical Quadric Error Metrics. *ACM Trans. Graph.* 32, 6 (2013), 178:1–178:12.

Jean-Marc Thiery, Émilie Guy, Tamy Boubekeur, and Elmar Eisemann. 2016. Animated Mesh Approximation with Sphere-Meshes. *ACM Trans. Graph.* 35, 3 (2016), 30:1–30:13.

G. Thomsen. 1924. Grundlagen der konformen flächentheorie. *Abh. Math. Sem. Univ. Hamburg* 3, 1 (1924), 31–56.

Anastasia Tkach, Mark Pauly, and Andrea Tagliasacchi. 2016. Sphere-Meshes for Real-Time Hand Modeling and Tracking. *ACM Trans. Graph.* 35, 6 (2016), 222:1–222:11.

Floor Verhoeven, Amir Vaxman, Tim Hoffmann, and Olga Sorkine-Hornung. 2022. Dev2PQ: Planar Quadrilateral Strip Remeshing of Developable Surfaces. *ACM Trans. Graph.* 41, 3, Article 29 (2022), 18 pages.

Rui Wang, Kun Zhou, John Snyder, Xinguo Liu, Hujun Bao, Qunsheng Peng, and Baining Guo. 2006. Variational sphere set approximation for solid objects. The Visual Computer, 22(9): 612-621. *The Visual Computer* 22 (09 2006), 612–621.

Jianhua Wu and Leif Kobbelt. 2005. Structure Recovery via Hybrid Variational Surface Approximation. *Computer Graphics Forum* 24 (2005).